Int. J. Fuzzy Syst.
https://doi.org/10.1007/s40815-018-0515-2

Dead-Zone Model-Based Adaptive Fuzzy Wavelet Control for Nonlinear Systems Including Input Saturation and Dynamic Uncertainties

Maryam Shahriari-Kahkeshi[1]

Received: 25 October 2017 / Revised: 11 June 2018 / Accepted: 14 June 2018

Abstract In this study, the problem of adaptive fuzzy wavelet network (FWN) control is investigated for nonlinear strict-feedback systems with unknown functions, unknown virtual control gains and unknown input saturation. An adaptive FWN as an adaptive nonlinear-in-parameter approximator is proposed to represent the model of the unknown functions. Saturation nonlinearity is described by the dead-zone operator-based model which does not require the bound of the saturated input to be known. Then, a novel control scheme is designed based on the adaptive FWN, the saturation model and the dynamic surface control approach. The proposed control scheme does not require any prior knowledge about input saturation, unknown dynamics and unknown virtual control gains. It simultaneously eliminates the "explosion of complexity" and "curse of dimensionality" problems; also, the design approach avoids the controller singularity problem completely without using projection algorithm. The stability analysis is studied using Lyapunov theorem; it shows that all signals of the resulting closed-loop system are uniformly ultimately bounded and the tracking error can be made small by proper selection of the design parameters. Comparing the simulation results of the proposed scheme with other control methods demonstrates the effectiveness and superior performance of the proposed scheme.

Keywords Adaptive fuzzy wavelet network · Dynamic surface control · Uncertain strict-feedback nonlinear system · Nonlinear-in-parameter approximator · Input saturation

✉ Maryam Shahriari-Kahkeshi
m.shahriyarikahkeshi@ec.iut.ac.ir

[1] Faculty of Engineering, Shahrekord University, Shahrekord, Iran

1 Introduction

Input saturation is one of the most important non-smooth nonlinear input constraints that usually appears in various practical systems such as electrical machines [1], robot manipulators [2], autonomous underwater vehicle [3, 4], MEMS [5, 6] and spacecraft [7, 8]. The presence of such nonlinearity should be explicitly considered in the control design schemes; otherwise, it may result in undesirable properties such as inaccuracy and degradation of the control performance or even, it may lead to instability of the closed-loop system. On the other hand, the most of practical control systems have nonlinear and uncertain behaviour [9]. Therefore, control of nonlinear uncertain systems with input saturation has attracted more attention, recently [10–17]. To compensate the saturation constraint in nonlinear systems, various robust and adaptive schemes have been developed, such as model predictive control [14], variable structure control [15], robust H_∞ control [16] and quantitative feedback theory [17].

Among the developed approaches, adaptive approximator-based backstepping techniques provide a systematic framework for designing of the control schemes [18]. They invoke conventional approximators such as neural networks (NNs) or fuzzy systems (FSs) to approximate the unknown functions of the system, and then, they employ adaptive techniques to provide systematic framework for controller design [13, 19–26]. So, they can handle a large class of uncertain nonlinear systems that their uncertainty does not satisfy the matching condition, or cannot be

Journal : Large 40815 | Dispatch : 20-6-2018 | Pages : 19
Article No. : 515 | □ LE | □ TYPESET
MS Code : IJFS-D-17-00702 | ☑ CP | ☑ DISK

linearly parameterized. Also, it is applicable to the cases that their uncertainty is completely unknown [27–31].

However, the aforementioned schemes based on the backstepping technique require the reference signal and its time derivatives up to nth order to be continuous and bounded; also, they suffer from two main difficulties. The first one is the "explosion of complexity" problem which is arisen because of repeated differentiations of nonlinear functions that appear in the design of virtual control inputs at each step. The other one is the "curse of dimensionality" which is arisen due to using NNs or FSs as a linear-in-parameter (LIP) approximator.

To overcome the "explosion of complexity" problem, the dynamic surface control (DSC) technique was proposed in [32]. It introduces a first-order low-pass filter at each step of the backstepping design procedure to avoid appearing of repeated derivatives of virtual control inputs and consequently to avoid "explosion of complexity" problem. Recently, some advanced DSC designs have been proposed. In [33], adaptive DSC scheme was proposed for a class of strict-feedback nonlinear systems with mismatched parametric uncertainties, where a composite learning scheme is used to update parametric uncertainties. A command-filtered backstepping adaptive control was proposed for a class of strict-feedback nonlinear systems with functional uncertainties in [34]. It proposes NN composite learning technique to guarantee convergence of NN weights to their ideal values without the persistent excitation condition. Design of composite adaptive DSC based on online recorded data was proposed in [35]. It uses both of tracking and prediction errors to update parametric estimates. Also, some of existing papers [36–40] have been proposed DSC-based control scheme for uncertain nonlinear systems with input saturation. In [36], a Gaussian error function-based saturation model was proposed and the Nussbaum-type gain function was used to deal with the unknown control direction. In [37], a hyperbolic tangent-based saturation model was used and a nonlinear disturbance observer was designed to estimate the effect of the disturbance. A Gaussian error-based model was proposed to describe the asymmetric saturation nonlinearity in [38], and then, a DSC-based control scheme was developed. Also, fuzzy-based DSC schemes were developed for uncertain nonlinear systems with input saturation in [39, 40].

The proposed works in [36–40] remedy the "explosion of complexity" problem, but they have two limitations. The first one is the need for the known bound of the saturated input, and the second one is the "curse of dimensionality" problem.

To overcome the first limitation, a dead-zone operator-based model was introduced to describe the saturation constraint and to develop adaptive backstepping controller for a class of nonlinear systems [41]. The considered system in [41] is not in the strict-feedback form; also, it does not solve the singularity problem. In [5], the stabilization problem of spacecraft rendezvous in the presence of the input saturation was investigated. In [42], a novel three-dimensional law based on input-to-state stability and nonlinear robust H_∞ filtering was proposed for interception of manoeuvring targets in the presence of input saturation. The robust constrained control was designed for MIMO nonlinear systems in [43]. In [5, 42, 43], it is assumed that the dynamics of the system and the virtual control gains are known and so, they do not use approximator-based control approach. The dead-zone model-based DSC control scheme was developed for stochastic nonlinear systems in [44]. However, the singularity problem and "curse of dimensionality" problems have not been solved.

The second limitation or "curse of dimensionality" problem is the result of using NNs or FSs as a LIP approximator to approximate unknown functions. When NNs or FSs are used as LIP approximators, the number of basis functions grows rapidly as the dimension of the argument vector of the functions increases. It results in a large number of basis functions, adjustable parameters and leads to large structure. Large structure requires long learning time and high computational load that make it a time-consuming process. Therefore, complexity of the controller grows drastically as the order of the system increases. Furthermore, as Barron shown in [45], the LIP approximator has integrated square approximation error of order $O(1/N)^{2/n}$ while the nonlinear-in-parameter (NIP) approximator has integrated square approximation error of order $O(1/N)$ where N is the number of basis functions and n is the dimension of the input to the function [45]. As it is inferred, the bound of the approximation error depends on n. So, in order to achieve the same approximation error for the same type of functions (to be approximated with dimension $n > 2$), the LIP approximator requires more basis functions and this leads to "curse of dimensionality", while for the same accuracy of approximation, the NIP approximator uses less number of basis functions than the LIP approximator and it can better avoid the curse of dimensionality problem [46]. So, compared with the LIP approximators, the NIP approximators can achieve the same quality of approximation with a smaller size of network, especially for higher-dimensional functions. In other words, the NIP approximator can achieve better quality of approximation with the same size of LIP approximator. AQ1

In this work, in order to avoid the "curse of dimensionality" problem (which is inevitable in the LIP approximator-based control schemes) and to avoid the singularity problem, the FWN as an adaptive NIP approximator is proposed to approximate unknown terms

Journal : Large 40815 | Dispatch : 20-6-2018 | Pages : 19
Article No. : 515 | LE | TYPESET
MS Code : IJFS-D-17-00702 | CP | DISK

of the system without any prior knowledge about the unknown functions and control gains. For the same approximation accuracy, application of the FWN as a NIP approximator is more simple than the LIP approximator (like FSs or NNs) in terms of the size, structure and number of parameters. However, theoretical analysis of the LIP approximator is simpler than the NIP one.

In the traditional adaptive fuzzy control, the consequent parts of the TSK-type fuzzy rules are represented by either a constant or a linear function of the input variable and a constant term. These consequent parts do not provide full mapping capabilities. TSK-type fuzzy systems do not have localizability. They model the global features of the process, and their convergence is generally slow. Also, they require a high number of rules for modelling of complex nonlinear processes with the desired accuracy. Increasing the number of the rules increases the number of neurons of the network. While, fuzzy wavelet network is a combination of fuzzy logic, wavelet theory and neural network. Contrary to the traditional TSK-type fuzzy networks, FWN uses wavelet functions in the consequent part of fuzzy rules and it can take advantages of the rigorous approximation theory of wavelet basis function expansion. Wavelet is a nonlinear function of input variables that analyse non-stationary signals and reveals their local details. Fuzzy logic reduces the complexity of the data and deals with uncertainty. Neural networks have self-learning characteristics that increase the accuracy of the model. So, their combination develops a system with fast learning capability that can describe uncertain nonlinear systems [47, 48].

This work proposes a dead-zone operator-based adaptive fuzzy wavelet dynamic surface control scheme for a class of uncertain nonlinear systems with unknown control gains and unknown input saturation. A dead-zone operator-based model is proposed to describe the saturation nonlinearity with unknown saturation bound. Adaptive FWN as an adaptive NIP approximator is proposed to model uncertain nonlinear dynamics. Then, the DSC approach is applied to develop a systematic design procedure for controller design. Stability analysis shows that all signals of the closed-loop system are uniformly ultimately bounded and the tracking error can be made small by the proper selection of the design parameters. The main contributions of this work are summarized as:

- Unlike the most of the existing schemes that use NNs or FSs as an adaptive LIP approximator, the proposed approach uses adaptive FWN as a NIP approximator and design adaptive learning laws to tune all of linear and nonlinear parameters of the network. So, it avoids the "curse of dimensionality" problem which is unavoidable in the adaptive LIP approximator-based control schemes developed in [18, 27–31, 36–40].
- Unlike [5, 38, 39, 43, 44], in this work, the virtual control gains are assumed to be unknown. Furthermore, the proposed design strategy avoids the singularity problem which has not been solved in many of the existing papers like [41, 44].
- Because of using DSC approach, the proposed scheme avoids the "explosion of complexity" problem which is inevitable in the backstepping-based schemes as in [18, 27–31].
- To eliminate the known bound assumption of the saturated input that exists in some of the existing works like [18, 36–40], a dead-zone operator-based model is employed to describe the saturation nonlinearity. Furthermore, the dead-zone model-based description describes various kinds of saturation such as hard-limit saturation and soft-limit saturation and it does not require the exact model of the input saturation.

The rest of this paper is organized as follows. Problem statement is stated in Sect. 2. Section 3 describes the FWN, briefly. Section 4 is devoted to the design of the proposed scheme, and it presents the main theorem. In Sect. 5, simulation and comparison results are presented to show the effectiveness and superior performance of the proposed scheme. Concluding remarks are given in Sect. 6. Finally, stability analysis of the closed-loop system is provided in "Appendix A".

2 Problem Statement

Consider a class of uncertain strict-feedback nonlinear systems with input saturation in the following form:

$$\begin{aligned} \dot{x}_i &= f_i(\boldsymbol{x}_i) + g_i(\boldsymbol{x}_i)x_{i+1}, \quad 1 \le i \le n-1 \\ \dot{x}_n &= f_n(\boldsymbol{x}_n) + g_n(\boldsymbol{x}_n)u(v) \\ y &= x_1 \end{aligned} \tag{1}$$

where $\boldsymbol{x}_i = [x_1 \quad x_2 \quad \ldots \quad x_i]^{\mathrm{T}} \in R^i$, $i = 1, 2, \ldots, n$, is the state vector, $y \in R$ is the output variable; function terms $f_i(\boldsymbol{x}_i) : R^i \to R$ and $g_i(\boldsymbol{x}_i) : R^i \to R$ $(i = 1, 2, \ldots, n)$ are unknown smooth nonlinear functions, g_i called the control gain function. $v \in R$ is the control input and $u(v) \in R$ is the saturated control input described as:

$$u(v) = \begin{cases} \operatorname{sign}(v)u_{\mathrm{sat}}, & |v| \ge u_{\mathrm{sat}} \\ v, & |v| < u_{\mathrm{sat}} \end{cases} \tag{2}$$

where u_{sat} is an unknown constant parameter. In this work, it is assumed that all state variables of the system (x_i, $i = 1, 2, \ldots, n$) are measurable.

Remark 1 The relationship between the applied control input u and the desired control input v has two sharp corners at $v = u_{\mathrm{sat}}$ and $v = -u_{\mathrm{sat}}$. So, the backstepping and the

Journal : Large 40815 | Dispatch : 20-6-2018 | Pages : 19
Article No. : 515 | LE | TYPESET
MS Code : IJFS-D-17-00702 | CP | DISK

DSC techniques cannot be directly applied to design the controller.

To deal with the saturation nonlinearity, the dead-zone operator-based model [41] is used to model the saturation function. This model is

$$u(v) = \rho_0 v - \int_0^R \rho(r)\mathrm{d}z_r(v)\mathrm{d}r \tag{3}$$

where $\rho(r)$ is a density function that satisfies $0 \le \rho(r) \le \rho_{\max}$ for $r > 0$ and $\rho(r) = 0$ for $r > R$; also, $\int_0^\infty r\rho(r)\mathrm{d}r < \infty$, and $\rho_0 = \int_0^R \rho(r)\mathrm{d}r$ is a positive constant, and $\mathrm{d}z_r(v) : R \to R$ is dead-zone operator that is defined as $\mathrm{d}z_r(v) = \max(v - r, \min(0, v + r))$. Also, the saturated value u_{sat} is obtained as follows:

$$u_{\mathrm{sat}} = \lim_{v\to\infty} u = \lim_{v\to\infty}\left(\rho_0 v - \int_0^R \rho(r)\mathrm{d}z_r(v)\mathrm{d}r\right) \tag{4}$$

Since $\lim_{v\to\infty} \mathrm{d}z_r(v) = \lim_{v\to\infty} (\max(v - r, \min(0, v + r)) = v - r$, so saturated value in (4) is calculates by

$$\begin{aligned} u_{\mathrm{sat}} &= \lim_{v\to\infty}\left(\rho_0 v - \int_0^R \rho(r)(v - r)\mathrm{d}r\right) \\ &= \lim_{v\to\infty}\int_0^R (\rho(r)v - \rho(r)(v - r))\mathrm{d}r \\ &= \lim_{v\to\infty}\int_0^R \rho(r)r\mathrm{d}r \end{aligned} \tag{5}$$

It is worth to note that different types of density functions that satisfy the mentioned properties can be used to model various forms of saturation nonlinearities.

In order to show the capabilities of the dead-zone operator-based model for describing saturation nonlinearity, an example is given. For this, consider the saturation nonlinearity (2) with $u_{\mathrm{sat}} = 2.5$ and the following $\rho(r)$:

$$\rho(r) = \begin{cases} 0.2 & 0 \le r \le R = 5 \\ 0 & r \ge 5 \end{cases} \tag{6}$$

Dead-zone operator $\mathrm{d}z_r(v)$ is shown in Fig. 1a; as it is seen from Fig. 1a, we have

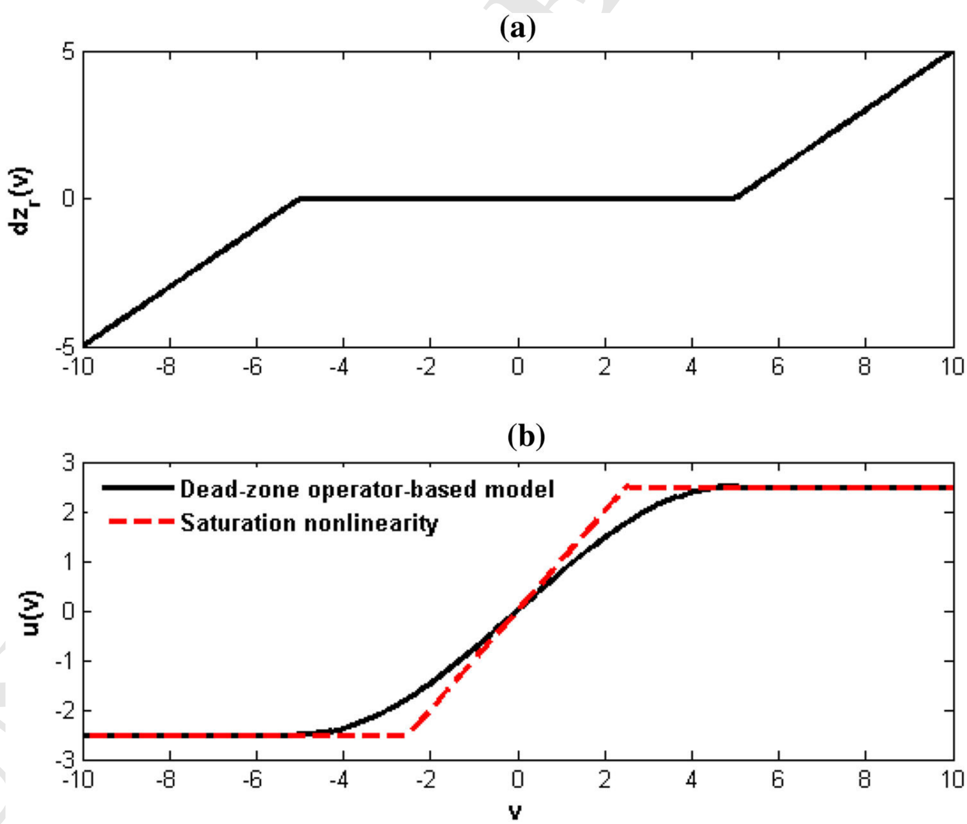

Fig. 1 **a** Dead-zone operator, **b** dead-zone operator-based model and saturation nonlinearity

Journal : Large 40815 Dispatch : 20-6-2018 Pages : 19
Article No. : 515 □ LE □ TYPESET
MS Code : IJFS-D-17-00702 ☑ CP ☑ DISK

$$\mathrm{d}z_r(v) = \begin{cases} v + r & v < -r \\ 0 & -r \le v \le r \\ v - r & v > r \end{cases}$$

Now, by substituting $\mathrm{d}z_r(v)$ into dead-zone operator-based model (3), $u(v)$ is obtained. Output of the dead-zone operator-based model and saturation nonlinearity are shown in Fig. 1b. As it is seen from Fig. 1b, the output of dead-zone operator-based model reaches the saturated values $u_{\text{sat}} = 2.5$ at $R = 5$. This verifies the capability of the dead-zone operator-based model to describe the saturation nonlinearity.

Now, considering (3), the nonlinear system (1) can be rewritten as:

$$\begin{aligned} \dot{x}_i &= f_i(\boldsymbol{x}_i) + g_i(\boldsymbol{x}_i)x_{i+1}, \quad 1 \le i \le n-1 \\ \dot{x}_n &= f_n(\boldsymbol{x}_n) + \beta(\boldsymbol{x}_n)v - g_n(\boldsymbol{x}_n)\int_0^R \rho(r)\mathrm{d}z_r(v)\mathrm{d}r \\ y &= x_1 \end{aligned} \tag{7}$$

where $\beta(\boldsymbol{x}_n) = \rho_0 g_n(\boldsymbol{x}_n)$.

Remark 2 Because of using the dead-zone operator-based model for saturation description, the saturation nonlinearity is represented in continuous differentiable form such that the DSC technique can be applied.

Assumption 1 The desired trajectory y_d is a sufficiently smooth function of t and y_d, $\dot{y}_d$ and $\ddot{y}_d$ are bounded, i.e. there exists a known positive constant B such that the set $\Pi := \{(y_d, \dot{y}_d, \ddot{y}_d) : y_d^2 + \dot{y}_d^2 + \ddot{y}_d^2 \le B\}$ is compact [32].

Assumption 2 The sign of g_i, $i = 1, 2, \ldots, n$ is known. Furthermore, there exist positive constants g_{li} and g_{hi} such that $g_{li} \le |g_i| \le g_{hi}$. Without losing generality, it is assumed that g_{li}, $i = 1, 2, \ldots, n$, is a positive constant.

Assumption 3 There exists a known positive constant g_i^d, $i = 1, 2, \ldots, n$ such that $|\dot{g}_i(.)| \le g_i^d$ in the compact set Ω_i.

Remark 3 Assumptions 2 and 3 imply that g_n and $\dot{g}_n$ are bounded. Furthermore, from the description of the dead-zone operator-based model ρ_0 is a positive constant. So, it is reasonable to conclude that $\beta(\boldsymbol{x}_n)$ satisfies $\beta_l \le |\beta(\boldsymbol{x}_n)| \le \beta_h$ and $|\dot{\beta}(\boldsymbol{x}_n)| \le \beta^d$.

The control objective is to design a dead-zone operator-based adaptive fuzzy wavelet dynamic surface control scheme such that the system output y tracks a desired trajectory y_d, and all signals of the closed-loop system remain uniformly ultimately bounded. Furthermore, the tracking error can be arbitrarily made small by proper selection of the design parameters.

Before the design of the proposed scheme, a brief description of the FWN as an adaptive NIP approximator is presented in the following section.

3 Fuzzy Wavelet Network as an Adaptive NIP Approximator

In this work, FWN is used as an adaptive NIP approximator to approximate the unknown continuous functions $h_i(z_i) : R^i \to R, \quad i = 1, \ldots, n$ by a set of N fuzzy rules in the following form [48]:

$$\begin{aligned} &\text{Rule } j: \text{If } z_1 \text{ is } A_1^j, \ldots \text{ and } z_i \text{ is } A_i^j, \\ &\text{Then } h_i^j = \theta_i^j \prod_{k=1}^{i} \varphi(\omega_{kj}(z_k - c_{kj})) \end{aligned} \tag{8}$$

where $j = 1, 2, \ldots, N$, $i = 1, 2, \ldots, n$, $z_1, \ldots, z_i$ are the input variables of the network, h_i^j is the output variable of the jth rule, $\theta_i^j \in R$ is the weight of the network, $\varphi(\omega_{kj}(z_k - c_{kj}))$ is a wavelet function that is obtained from translation and dilation of the single mother wavelet function; also, A_i^j represents the linguistic term that is characterized by the Gaussian-type fuzzy membership function as:

$$\mu_{A_i^j}(z_i) = \exp\left(-(\omega_{ij}(z_i - c_{ij}))^2\right) \tag{9}$$

where ω_{ij} and c_{ij} denote the inverse of width and centre of the Gaussian membership function that are chosen as the same as dilation and translation parameters of wavelet functions, respectively. Combination of the firing strength of the jth rule as $\prod_{k=1}^{i} \mu_{A_k^j}(z_k)$ and wavelet function $\prod_{k=1}^{i} \varphi(\omega_{kj}(z_k - c_{kj}))$ forms the jth fuzzy wavelet basis function ψ_j as [48]:

$$\begin{aligned} \psi_j(z_i, \boldsymbol{c}_j, \boldsymbol{\omega}_j) = &\left(\prod_{k=1}^{i} \exp\left(-(\omega_{kj}(z_k - c_{kj}))^2\right)\right) \\ &\times \left(\prod_{k=1}^{i} \varphi(\omega_{kj}(z_k - c_{kj}))\right) \end{aligned} \tag{10}$$

The output of the above FWN is computed as:

$$h_i(z_i, \boldsymbol{c}_i, \boldsymbol{\omega}_i, \boldsymbol{\theta}_i) = \sum_{j=1}^{N} \theta_i^j \psi_j(z_i, \boldsymbol{c}_i, \boldsymbol{\omega}_i) \tag{11}$$

where $i = 1, 2, \ldots, n$, $\boldsymbol{c}_i = [c_{i1}, c_{i2}, \ldots, c_{iN}]^{\mathrm{T}} \in R^N$ is the translation parameter vector and $\boldsymbol{\omega}_i = [\omega_{i1}, \omega_{i2}, \ldots, \omega_{iN}]^{\mathrm{T}} \in R^N$ is the dilation parameter vector. For simplicity, the output of FWN in (11) is expressed as:

$$h_i(z_i, \boldsymbol{c}_i, \boldsymbol{\omega}_i, \boldsymbol{\theta}_i) = \boldsymbol{\theta}_i^{\mathrm{T}} \boldsymbol{\psi}_j(z_i, \boldsymbol{c}_i, \boldsymbol{\omega}_i) \tag{12}$$

where $\boldsymbol{\psi}_j = [\psi_1, \ldots, \psi_N]^{\mathrm{T}} \in R^N$ denote the vector of the fuzzy wavelet basis functions and $\boldsymbol{\theta}_i = [\theta_i^1, \ldots, \theta_i^N]^{\mathrm{T}} \in R^N$ is the weight vector.

According to the universal approximation property, the FWN can approximate any continuous function $h_i(z_i)$

Journal : Large 40815 | Dispatch : 20-6-2018 | Pages : 19
Article No. : 515 | ☐ LE | ☐ TYPESET
MS Code : IJFS-D-17-00702 | ☑ CP | ☑ DISK

defined over a compact set $\Omega_{z_i} \subset R^i$ to any arbitrary accuracy δ_i^* [48]. So, there exist an ideal weight vector $\boldsymbol{\theta}_i^*$ and ideal dilation and translation vectors $\boldsymbol{\omega}_i^*$ and $\boldsymbol{c}_i^*$ such that

$$h_i(z_i) = \boldsymbol{\theta}_i^{*\mathrm{T}} \boldsymbol{\psi}\left(z_i, \boldsymbol{c}_j^*, \boldsymbol{\omega}_j^*\right) + \delta_i^*(z_i) \tag{13}$$

where $\delta_i^*(z_i)$ is the approximation error that satisfies $\left|\delta_i^*(z_i)\right| \leq \bar{\delta}_i$ [48]. According to the universal approximation theorem, $\boldsymbol{\theta}_i^*, \boldsymbol{c}_i^*, \boldsymbol{\omega}_i^*$ are bounded. So, the ideal parameter vectors are norm bounded.

Assumption 4 The norm of the ideal parameter vectors is bounded; so, there exist unknown constants $\bar{\theta}_i$, $\bar{c}_i$ and $\bar{\omega}_i$ such that $\boldsymbol{\theta}_i^{*\mathrm{T}} \boldsymbol{\theta}_i^* \leq \bar{\theta}_i$, $\boldsymbol{c}_i^{*\mathrm{T}} \boldsymbol{c}_i^* \leq \bar{c}_i$ and $\boldsymbol{\omega}_i^{*\mathrm{T}} \boldsymbol{\omega}_i^* \leq \bar{\omega}_i$. However, the ideal parameters are unknown. So, it is necessary to estimate them. In the following, $\hat{\boldsymbol{\theta}}_i$, $\hat{\boldsymbol{c}}_i$ and $\hat{\boldsymbol{\omega}}_i$ denote the estimation of ideal parameters $\boldsymbol{\theta}_i^*$, $\boldsymbol{c}_i^*$ and $\boldsymbol{\omega}_i^*$, respectively. So, the approximated function is defined as:

$$\hat{h}_i(z_i) = \hat{\boldsymbol{\theta}}_i^{\mathrm{T}} \boldsymbol{\psi}_j\left(z_i, \hat{\boldsymbol{c}}_j, \hat{\boldsymbol{\omega}}_j\right) \tag{14}$$

The structure of the FWN is shown in Fig. 2.

In the following, for ease of notation, ideal and estimated basis functions $\boldsymbol{\psi}_j\left(\boldsymbol{x}_i, \boldsymbol{c}_j^*, \boldsymbol{\omega}_j^*\right)$ and $\boldsymbol{\psi}_j\left(\boldsymbol{x}_i, \hat{\boldsymbol{c}}_j, \hat{\boldsymbol{\omega}}_j\right)$ are represented by $\boldsymbol{\psi}_j^*$ and $\hat{\boldsymbol{\psi}}_j$, respectively.

Remark 4 It must be noted that the designed adaptive FWN as a NIP approximator can be used in both online and off-line applications. However, in this work, it is used online and requires no prior knowledge or off-line learning and all of its parameters are adjusted online based on the adaptive laws.

4 Design of the Proposed Control Scheme

In this section, in order to avoid the problems of "explosion of complexity" and "curse of dimensionality", the proposed adaptive FWN-based DSC scheme is designed for the uncertain nonlinear system (7) in the presence of input saturation. The design procedure is described as follows:

Step 1 The first error surface or tracking error is defined as:

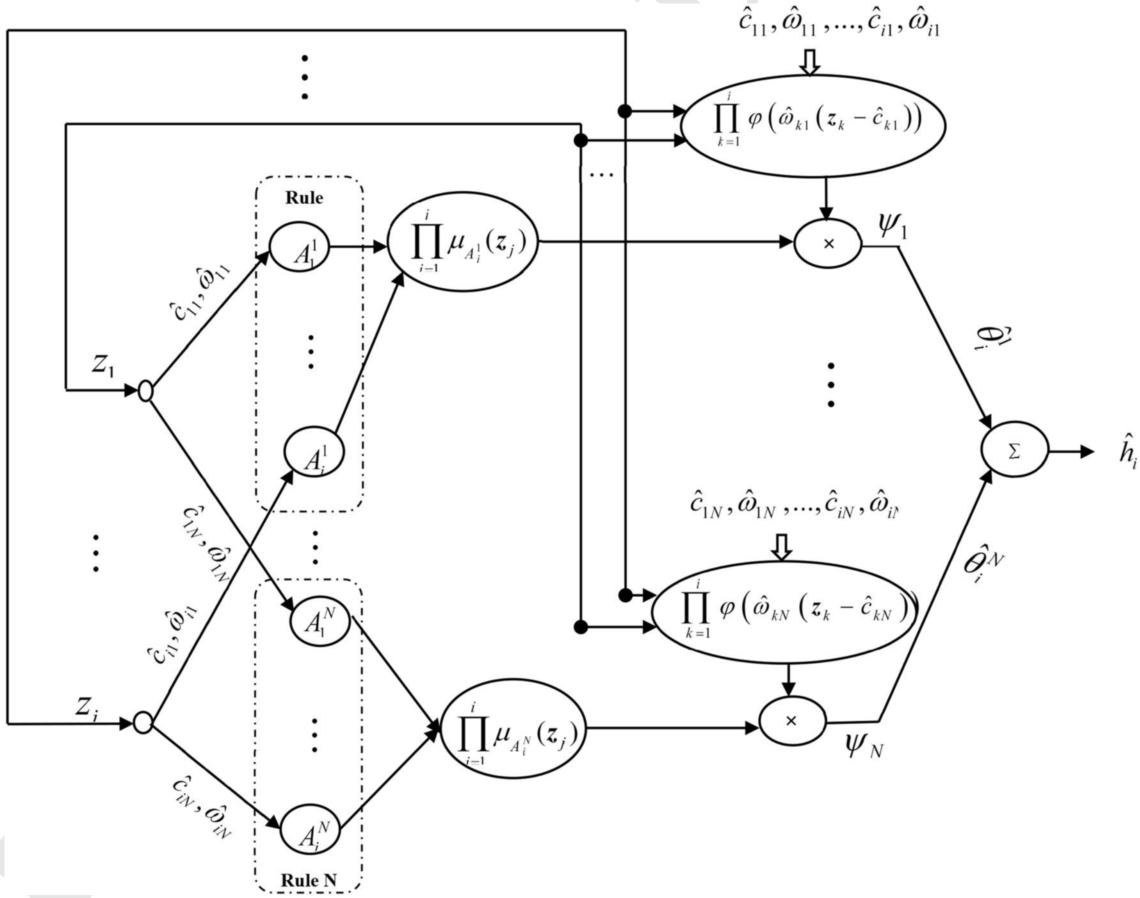

Fig. 2 Structure of the adaptive fuzzy wavelet network

Journal : Large 40815 | Dispatch : 20-6-2018 | Pages : 19
Article No. : 515 | LE | TYPESET
MS Code : IJFS-D-17-00702 | CP | DISK

$$e_1 = y - y_d \tag{15}$$

Invoking (7) and differentiating (15) with respect to time yields:

$$\dot{e}_1 = f_1 + g_1 x_2 - \dot{y}_d \tag{16}$$

Assuming x_2 as a virtual control input, the desired feedback control is designed as:

$$v_2^* = -k_1 e_1 - \frac{1}{g_1}(f_1 - \dot{y}_d) \tag{17}$$

where k_1 is a positive design constant; Since g_1 and f_1 are unknown smooth functions of x_1, the desired feedback control input v_2^* in (17) cannot be implemented in practice.

Let us define $h_1(z_1) = (1/g_1)(f_1 - \dot{y}_d)$ where $z_1 = [x_1, \dot{y}_d]^{\mathrm{T}}$ and employ adaptive FWN to approximate $h_1(z_1)$. Considering (13), v_2^* in (16) can be expressed as:

$$v_2^* = -k_1 e_1 - \boldsymbol{\theta}_1^{*\mathrm{T}} \boldsymbol{\psi}\left(z_1, \boldsymbol{c}_1^*, \boldsymbol{\omega}_1^*\right) - \delta_1^* \tag{18}$$

Since the ideal parameters $\boldsymbol{\theta}_1^*$, $\boldsymbol{c}_1^*$, $\boldsymbol{\omega}_1^*$ and the approximation error δ_1^* are unknown, the virtual control law is proposed as:

$$v_2 = -k_1 e_1 - \hat{\boldsymbol{\theta}}_1^{\mathrm{T}} \boldsymbol{\psi}(z_1, \hat{\boldsymbol{c}}_1, \hat{\boldsymbol{\omega}}_1) \tag{19}$$

where $\hat{\boldsymbol{\theta}}_1$, $\hat{\boldsymbol{c}}_1$, $\hat{\boldsymbol{\omega}}_1$ are the estimations of $\boldsymbol{\theta}_1^*$, $\boldsymbol{c}_1^*$, $\boldsymbol{\omega}_1^*$ which are adjusted by:

$$\begin{aligned}
\dot{\hat{\boldsymbol{\theta}}}_1 &= \gamma_1\left(\left(\hat{\boldsymbol{\psi}}_1 - A_1^{\mathrm{T}}\hat{\boldsymbol{\omega}}_1 - B_1^{\mathrm{T}}\hat{\boldsymbol{c}}_1\right)e_1 - \sigma\hat{\boldsymbol{\theta}}_1\right)\\
\dot{\hat{\boldsymbol{c}}}_1 &= \gamma_2\left(B_1\hat{\boldsymbol{\theta}}_1 e_1 - \sigma\hat{\boldsymbol{c}}_1\right)\\
\dot{\hat{\boldsymbol{\omega}}}_1 &= \gamma_3\left(A_1\hat{\boldsymbol{\theta}}_1 e_1 - \sigma\hat{\boldsymbol{\omega}}_1\right)
\end{aligned} \tag{20}$$

where $A_1 = \left(\frac{\partial\psi_1}{\partial\omega_1}\right)\Big|_{\omega_1=\hat{\omega}_1}$ and $B_1 = \left(\frac{\partial\psi_1}{\partial c_1}\right)\Big|_{c_1=\hat{c}_1}$, γ_1, γ_2 and γ_3 are learning parameters and $\sigma > 0$ is a design parameter.

To avoid repeated differentiating of v_2 which leads to the "explosion of complexity" problem, the DSC technique is employed. Let v_2 pass through the first-order filter with time constant τ_2 :

$$\tau_2 \dot{v}_{2f} + v_{2f} = v_2\ , \ v_{2f}(0) = v_2(0) \tag{21}$$

Defining $e_2 = x_2 - v_{2f}$ and $\eta_2 = v_{2f} - v_2$ results in $x_2 = e_2 + \eta_2 + v_2$. So, (16) can be written as:

$$\begin{aligned}
\dot{e}_1 &= f_1 + g_1(e_2 + \eta_2 + v_2) - \dot{y}_d\\
&= g_1 h_1 + g_1(e_2 + \eta_2 + v_2)\\
&= g_1\left(e_2 + \eta_2 - k_1 e_1 + \tilde{h}_1\right)
\end{aligned} \tag{22}$$

where $\tilde{h}_1 = \boldsymbol{\theta}_1^{*\mathrm{T}}\boldsymbol{\psi}_1^* + \delta_1^* - \hat{\boldsymbol{\theta}}_1^{\mathrm{T}}\hat{\boldsymbol{\psi}}_1$ is the approximation error.

Differentiating η_2 with respect to time and substituting (21) in it and using $\eta_2 = v_{2f} - v_2$ results in:

$$\begin{aligned}
\dot{\eta}_2 &= \dot{v}_{2f} - \dot{v}_2 = \frac{v_2 - v_{2f}}{\tau_2} - \dot{v}_2 = -\frac{\eta_2}{\tau_2}\\
&\quad - \left(\frac{\partial v_2}{\partial e_1}\dot{e}_1 + \frac{\partial v_2}{\partial \psi_1}\frac{\partial \psi_1}{\partial x_1}\dot{x}_1 + \frac{\partial v_2}{\partial \psi_1}\frac{\partial \psi_1}{\partial y_d}\dot{y}_d\right.\\
&\quad \left. + \frac{\partial v_2}{\partial \psi_1}\frac{\partial \psi_1}{\partial \hat{\boldsymbol{\theta}}_1}\dot{\hat{\boldsymbol{\theta}}}_1 - \frac{\partial v_2}{\partial \psi_1}\frac{\partial \psi_1}{\partial \hat{c}_1}\dot{\hat{\boldsymbol{c}}}_1 - \frac{\partial v_2}{\partial \psi_1}\frac{\partial \psi_1}{\partial \hat{\omega}_1}\dot{\hat{\boldsymbol{\omega}}}_1\right)\\
&= -\frac{\eta_2}{\tau_2} + M_2\left(e_1, e_2, \eta_2, \hat{\boldsymbol{\theta}}_1, \hat{\boldsymbol{c}}_1, \hat{\boldsymbol{\omega}}_1, y_d, \dot{y}_d\right)
\end{aligned} \tag{23}$$

where $M_2(.)$ is a continues function. For any B and p, the sets $\Pi := \left\{(y_d, \dot{y}_d, \ddot{y}_d) : y_d^2 + \dot{y}_d^2 + \ddot{y}_d^2 \le B\right\}$ and $\Pi_1 := \left\{e_1^2 + e_2^2 + \eta_2^2 + \tilde{\boldsymbol{\theta}}_1^{\mathrm{T}}\tilde{\boldsymbol{\theta}}_1 + \tilde{\boldsymbol{c}}_1^{\mathrm{T}}\tilde{\boldsymbol{c}}_1 + \tilde{\boldsymbol{\omega}}_1^{\mathrm{T}}\tilde{\boldsymbol{\omega}}_1 \le 2p\right\}$ are compact in R^3 and R^{3N+3}, respectively. Thus, $\Pi \times \Pi_1$ is also compact. Considering continuous property, the function $M_2(.)$ has a maximum bound $\bar{M}_2$ for the given initial condition in the compact set $\Pi \times \Pi_1$ [21].

Step i $(2 \le i \le n-1)$: In the ith step, the ith error surface is defined as

$$e_i = x_i - v_{if} \tag{24}$$

where $v_{if} \in R$ is obtained from the step $i-1$. Considering (7) and differentiating e_i with respect to time results in:

$$\dot{e}_i = f_i + g_i x_{i+1} - \dot{v}_{if} \tag{25}$$

Assuming x_{i+1} as a virtual control input, the desired feedback control v_{i+1}^* is designed as:

$$v_{i+1}^* = -k_i e_i - \frac{1}{g_i}\left(f_i - \dot{v}_{if}\right) \tag{26}$$

where k_i is a positive design parameter, f_i and g_i are unknown smooth functions of $\boldsymbol{x}_i$. Let us define $h_i(z_i) = (1/g_i)\left(f_i - \dot{v}_{if}\right)$ with $z_i = [\boldsymbol{x}_i, \dot{v}_{if}]^{\mathrm{T}}$ where $\boldsymbol{x}_i = [x_1, x_2, \ldots, x_i]^{\mathrm{T}}$. By applying adaptive FWN to approximate $h_i(z_i)$ and considering (13), v_{i+1}^* in (26) can be written as

$$v_{i+1}^* = -k_i e_i - \boldsymbol{\theta}_i^{*\mathrm{T}}\boldsymbol{\psi}\left(z_i, \boldsymbol{c}_i^*, \boldsymbol{\omega}_i^*\right) - \delta_i^* \tag{27}$$

Since ideal parameters $\boldsymbol{\theta}_i^*, \boldsymbol{c}_i^*, \boldsymbol{\omega}_i^*$ and approximation error δ_i^* are unknown, the virtual control law is proposed as

$$v_{i+1} = -k_i e_i - \hat{\boldsymbol{\theta}}_i^{\mathrm{T}}\boldsymbol{\psi}(z_i, \hat{\boldsymbol{c}}_i, \hat{\boldsymbol{\omega}}_i) \tag{28}$$

where $\hat{\boldsymbol{\theta}}_i$, $\hat{\boldsymbol{c}}_i$, $\hat{\boldsymbol{\omega}}_i$ denote the estimation of $\boldsymbol{\theta}_i^*$, $\boldsymbol{c}_i^*$, $\boldsymbol{\omega}_i^*$ which are adjusted by the following adaptive learning laws

Journal : Large 40815 | Dispatch : 20-6-2018 | Pages : 19
Article No. : 515 | LE | TYPESET
MS Code : IJFS-D-17-00702 | CP | DISK

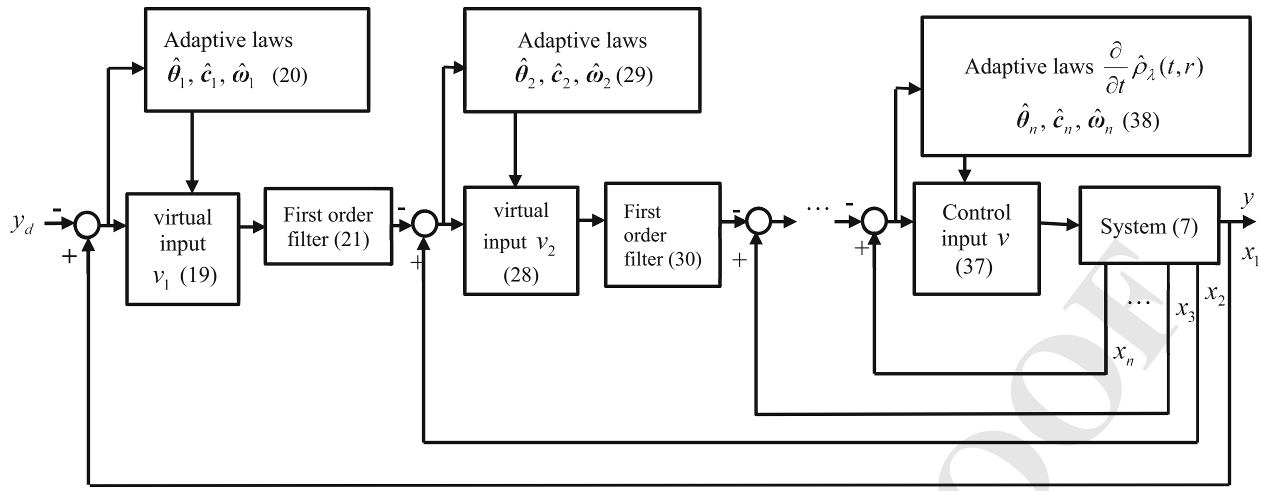

Fig. 3 Block diagram of the proposed controller

$$
\begin{aligned}
\dot{\hat{\boldsymbol{\theta}}}_i &= \gamma_1\left(\left(\hat{\boldsymbol{\psi}}_i - A_i^{\mathrm{T}}\hat{\boldsymbol{\omega}}_i - B_i^{\mathrm{T}}\hat{\boldsymbol{c}}_i\right)e_i - \sigma\hat{\boldsymbol{\theta}}_i\right)\\
\dot{\hat{\boldsymbol{c}}}_i &= \gamma_2\left(B_i\hat{\boldsymbol{\theta}}_i e_i - \sigma\hat{\boldsymbol{c}}_i\right)\\
\dot{\hat{\boldsymbol{\omega}}}_i &= \gamma_3\left(A_i\hat{\boldsymbol{\theta}}_i e_i - \sigma\hat{\boldsymbol{\omega}}_i\right)
\end{aligned}
\tag{29}
$$

where $A_i = \left(\frac{\partial\psi_i}{\partial\omega_i}\right)\Big|_{\omega_i=\hat{\omega}_i}$, $B_i = \left(\frac{\partial\psi_i}{\partial c_i}\right)\Big|_{c_i=\hat{c}_i}$. Let v_{i+1} pass through the first-order filter with time constant τ_{i+1} as

$$\tau_{i+1}\dot{v}_{(i+1)f} + v_{(i+1)f} = v_{i+1}\ ,\ v_{(i+1)f}(0) = v_{i+1}(0) \tag{30}$$

Defining $e_{i+1} = x_{i+1} - v_{(i+1)f}$ and $\eta_{i+1} = v_{(i+1)f} - v_{i+1}$ gives $x_{i+1} = e_{i+1} + \eta_{i+1} + v_{i+1}$. So, (25) can be written as

$$
\begin{aligned}
\dot{e}_i &= f_i + g_i(e_{i+1} + \eta_{i+1} + v_{i+1}) - \dot{v}_{(i+1)f}\\
&= g_i h_i + g_i(e_{i+1} + \eta_{i+1} + v_{i+1})\\
&= g_i(e_{i+1} + \eta_{i+1} - k_i e_i + \tilde{h}_i)
\end{aligned}
\tag{31}
$$

where $\tilde{h}_i = \boldsymbol{\theta}_i^{*\mathrm{T}}\boldsymbol{\psi}_i^* + \delta_i^* - \hat{\boldsymbol{\theta}}_i^{\mathrm{T}}\hat{\boldsymbol{\psi}}_i$ is the approximation error.

Differentiating η_{i+1} with respect to time and substituting (30) in it and using $\eta_{i+1} = v_{(i+1)f} - v_{i+1}$ results in:

$$
\begin{aligned}
\dot{\eta}_{i+1} = \dot{v}_{(i+1)f} - \dot{v}_{1+1} = &-\frac{\eta_{i+1}}{\tau_{i+1}}\\
&-\left(\frac{\partial v_{i+1}}{\partial e_i}\dot{e}_i + \sum_{j=1}^{i}\left(\frac{\partial v_{i+1}}{\partial\psi_j}\frac{\partial\psi_j}{\partial x_j}\dot{x}_j + \frac{\partial v_{i+1}}{\partial\psi_j}\frac{\partial\psi_j}{\partial\dot{v}_{(j+1)f}}\ddot{v}_{(j+1)f}\right.\right.\\
&\left.\left.+\frac{\partial v_{i+1}}{\partial\psi_j}\frac{\partial\psi_j}{\partial\hat{\boldsymbol{\theta}}_j}\dot{\hat{\boldsymbol{\theta}}}_j + \frac{\partial v_{i+1}}{\partial\psi_j}\frac{\partial\psi_j}{\partial\hat{\boldsymbol{c}}_j}\dot{\hat{\boldsymbol{c}}}_j + \frac{\partial v_{i+1}}{\partial\psi_j}\frac{\partial\psi_j}{\partial\hat{\boldsymbol{\omega}}_j}\dot{\hat{\boldsymbol{\omega}}}_j\right)\right)\\
= &-\frac{\eta_{i+1}}{\tau_{i+1}} + M_{i+1}(.)
\end{aligned}
\tag{32}
$$

where $M_{i+1}(.)$ is a continues function and has a maximum bound $\bar{M}_{i+1}$ [21].

Step n In the final step, the actual control input v will be deigned. The error surface is defined as

$$e_n = x_n - v_{nf} \tag{33}$$

where v_n is obtained from the step $n-1$. Let $\rho_\lambda(r) := \rho(r)/\rho_0$; then, the time derivative of e_n is

$$\dot{e}_n = \dot{x}_n - \dot{v}_{nf} = \beta v + f_n - \dot{v}_{nf} - \beta\int_0^R \rho_\lambda(r)\mathrm{d}z_r(v)\mathrm{d}r \tag{34}$$

The ideal control input is constructed as

$$v^* = -\frac{1}{\beta}\left(f_n - \dot{v}_{nf}\right) - k_n e_n + \int_0^R \rho_\lambda(r)\mathrm{d}z_r(v)\mathrm{d}r \tag{35}$$

where $k_n > 0$ is a design parameter and f_n, g_n, β and $\rho_\lambda(r)$ are unknown. Let us define $h_n(z_n) = \frac{1}{\beta}\left(f_n - \dot{v}_{nf}\right)$ where $z_n = [\boldsymbol{x}_n, \dot{v}_{nf}]^{\mathrm{T}}$ and $\boldsymbol{x}_n = [x_1, x_2, \ldots, x_n]^{\mathrm{T}}$. Considering (13), the ideal control input is designed as

$$
\begin{aligned}
v^* = &-\boldsymbol{\theta}_n^{*\mathrm{T}}\boldsymbol{\psi}\left(z_n, \boldsymbol{c}_j^*, \boldsymbol{\omega}_j^*\right) - \delta_n^*(z_n) - k_n e_n\\
&+\int_0^R \rho_\lambda(r)\mathrm{d}z_r(v)\mathrm{d}r
\end{aligned}
\tag{36}
$$

Since ideal parameters $\boldsymbol{c}_n^*$, $\boldsymbol{\omega}_n^*$, $\boldsymbol{\theta}_n^*$ and $\rho_\lambda(r)$ are unknown, it is not possible to implement the ideal control input v^*. So, the actual control input v is proposed as

$$v = -\hat{\boldsymbol{\theta}}_n^{\mathrm{T}}\boldsymbol{\psi}(z_n, \hat{\boldsymbol{c}}_n, \hat{\boldsymbol{\omega}}_n) - k_n e_n + \int_0^R \hat{\rho}_\lambda(r,t)\mathrm{d}z_r(v)\mathrm{d}r \tag{37}$$

where $\hat{\boldsymbol{c}}_n$, $\hat{\boldsymbol{\omega}}_n$, $\hat{\boldsymbol{\theta}}_n$ and $\hat{\rho}_\lambda(r,t)$ denote the estimation of

Journal : Large 40815 | Dispatch : 20-6-2018 | Pages : 19
Article No. : 515 | LE | TYPESET
MS Code : IJFS-D-17-00702 | CP | DISK

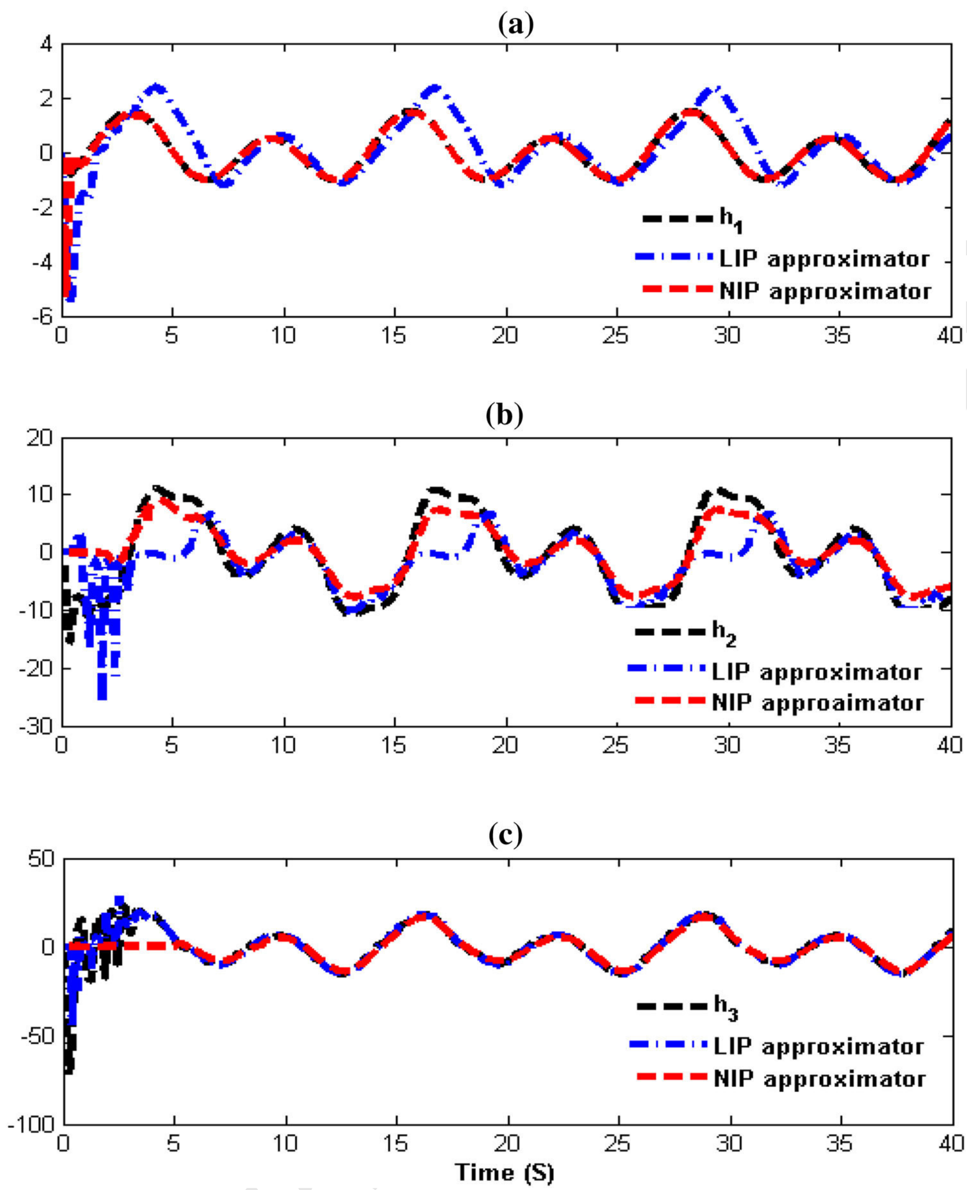

Fig. 4 Uncertain functions $h_i(z_i)$ for $i = 1, 2, 3$ and their estimation using LIP and NIP approximator, **a** $h_1(z_1)$ and its approximation, **b** $h_2(z_2)$ and its approximation, **c** $h_3(z_3)$ and its approximation

$\boldsymbol{c}_n^*$, $\boldsymbol{\omega}_n^*$, $\boldsymbol{\theta}_n^*$ and $\rho_\lambda(r)$, respectively, and they are adjusted based on the following adaptive learning laws

$$\begin{aligned}
\dot{\hat{\boldsymbol{\theta}}}_n &= \gamma_1\left(\left(\hat{\boldsymbol{\psi}}_n - A_n^{\mathrm{T}}\hat{\boldsymbol{\omega}}_n - B_n^{\mathrm{T}}\hat{\boldsymbol{c}}_n\right)e_n - \sigma\hat{\boldsymbol{\theta}}_n\right)\\
\dot{\hat{\boldsymbol{c}}}_n &= \gamma_2\left(B_n\hat{\boldsymbol{\theta}}_n e_n - \sigma\hat{\boldsymbol{c}}_n\right)\\
\dot{\hat{\boldsymbol{\omega}}}_n &= \gamma_3\left(A_n\hat{\boldsymbol{\theta}}_n e_n - \sigma\hat{\boldsymbol{\omega}}_n\right)\\
\frac{\partial}{\partial t}\hat{\rho}_\lambda(t,r) &= \gamma_\rho\left(-e_n \mathrm{d}z_r(v) - \sigma_\rho\hat{\rho}_\lambda(t,r)\right)
\end{aligned} \tag{38}$$

where γ_ρ and σ_ρ are the design parameters, $A_n = \left(\frac{\partial\psi_n}{\partial\omega_n}\right)\Big|_{\boldsymbol{\omega}_n=\hat{\boldsymbol{\omega}}_n}$, $B_n = \left(\frac{\partial\psi_n}{\partial c_n}\right)\Big|_{\boldsymbol{c}_n=\hat{\boldsymbol{c}}_n}$. Considering (38), the error dynamics in (34) is obtained as

$$\dot{e}_n = \beta\left(-k_n e_n + \int_0^R (\hat{\rho}_\lambda(r,t) - \rho_\lambda(r))\mathrm{d}z_r(v)\mathrm{d}r + \tilde{h}_n\right) \tag{39}$$

where $\tilde{h}_n = \boldsymbol{\theta}_n^{*\mathrm{T}}\boldsymbol{\psi}_n^* + \delta_n^* - \hat{\boldsymbol{\theta}}_n^{\mathrm{T}}\hat{\boldsymbol{\psi}}_n$ is the approximation error.The block diagram of the proposed scheme is shown in Fig. 3. Also, the following theorem summarizes the design of proposed controller.

Theorem 1 *Consider the class of strict-feedback nonlinear system (1) with the input saturation and dynamic uncertainties. The dead-zone operator-based model (3) is used to describe the saturation nonlinearity and the*

Journal : Large 40815 | Dispatch : 20-6-2018 | Pages : 19
Article No. : 515 | ☐ LE | ☐ TYPESET
MS Code : IJFS-D-17-00702 | ☑ CP | ☑ DISK

adaptive FWN as an adaptive NIP approximator is designed to model the unknown terms of the system in the controller design. Given any positive number p, for all initial conditions satisfying $\Pi_n := \sum_{i=1}^{n-1}\left(\frac{1}{g_i}e_i^2+\frac{1}{\gamma_1}\tilde{\boldsymbol{\theta}}_i^{\mathrm{T}}\tilde{\boldsymbol{\theta}}_i+\frac{1}{\gamma_2}\tilde{\boldsymbol{c}}_i^{\mathrm{T}}\tilde{\boldsymbol{c}}_i+\frac{1}{\gamma_3}\tilde{\boldsymbol{\omega}}_i^{\mathrm{T}}\tilde{\boldsymbol{\omega}}_i\right)+\frac{1}{\beta}e_n^2+\sum_{i=1}^{n-1}\eta_{i+1}^2+\frac{1}{\gamma_\rho}\int_0^R\tilde{\rho}_\lambda^2(r,t)\mathrm{d}r \leq 2p$ *the proposed scheme guarantees that all signals of the closed-loop system are uniformly ultimately bounded. Furthermore, the tracking error can be made small by proper choice of the design parameters.*

Proof Proof of Theorem 1 is presented in "Appendix A".

Remark 5 To implement the control law (37), the integral term is approximated as

$$\int_0^R \hat{\rho}_\lambda(r,t)\mathrm{d}z_r(v)\mathrm{d}r \cong \sum_{i=1}^{M}\hat{\rho}_\lambda(i\Delta r,t)\Delta r \tag{40}$$

in which Δr is a step size and $M = R/\Delta r$. Small values of Δr result in accurate estimation of integral term, but they require more computation [41]. Therefore, there is a trade of between approximation accuracy and computational complexity.

Remark 6 Considering $\boldsymbol{z}_i = [\boldsymbol{x}_i, \dot{v}_{if}]^{\mathrm{T}}$ for $2 \leq i \leq n$, the dimension of the input argument of the function $h_i(\boldsymbol{z}_i)$ is greater than 2; So, to achieve the same approximation accuracy for the same function $h_i(\boldsymbol{z}_i)$, the LIP approximator requires more basis functions than the proposed FWN as a NIP approximator. Therefore, applying the LIP approximator leads to the increase in the size and adjustable parameters of the controller and consequently results in the "curse of dimensionality" problem.

Remark 7 It is worth to note that the bound of $M_{i+1}(.)$ for $i = 1,\ldots,n-1$ is only required for stability analysis of the closed-loop system and design of the proposed controller does not require estimating its maximum value.

5 Simulation Results

In this section, the one-link manipulator with a brush DC motor is considered to illustrate the effectiveness and performance of the proposed scheme. Simulation and comparison results are provided to confirm the effectiveness and superior performance of the proposed scheme.

The dynamic model of the considered system is given by the following differential equations [49]:

$$\begin{cases} D\ddot{q} + B\dot{q} + N\sin(q) = I \\ M_m\dot{I} + H_mI = E - K_m\dot{q} \end{cases} \tag{41}$$

where q, $\dot{q}$ and $\ddot{q}$ denote the link angular position, velocity and acceleration, respectively. I is the motor current and E is the input voltage. The parameter values with appropriate units were set to $D = 1$, $M_m = 0.1$, $B = 1$, $K_m = 10$, $H_m = 0.5$ and $N = 10$ [37]. Let us define $x_1 = q$, $x_2 = \dot{q}$, $x_3 = I$, $u = E$, and $y = q$. Considering the input saturation, the state-space model of (41) can be expressed as

$$\begin{aligned} \dot{x}_1 &= x_2 \\ \dot{x}_2 &= (-N\sin(x_1) - Bx_2)/D + (1/D)x_3 \\ \dot{x}_3 &= (-K_mx_2 - Hx_3)/M + (1/M)u(v) \\ y &= x_1 \end{aligned} \tag{42}$$

where the saturation nonlinearity $u(v)$ is described by (2) and $u_{\mathrm{sat}} = 50$.

To show the effectiveness of the proposed controller, the proposed scheme in this work, the conventional DSC controller and the NN-based DSC approach [37] were applied to (42). In the following, each scheme is explained. However, for the conventional controller, the saturation phenomenon in (42) has not been considered.

- *The proposed controller*
  The first step for designing the proposed controller is to construct adaptive FWN as an adaptive NIP approximator. For this, three adaptive FWNs were constructed to approximate uncertain functions $h_1(z_1) = -\dot{y}_d$, $h_2(z_2) = \left(f_2(\boldsymbol{x}_2) - \dot{v}_{2f}\right)/g_2$, and $h_3(z_3) = \left(f_3(\boldsymbol{x}_3) - \dot{v}_{3f}\right)/g_3$ where $z_1 = \dot{y}_d$, $z_2 = [x_1 \quad x_2 \quad \dot{v}_{2f}]^T$, and $z_3 = [x_2 \quad x_3 \quad \dot{v}_{3f}]^T$ for controller design. In the following, z_1, z_2 and z_3 denote the inputs and $\hat{h}_1(z_1)$, $\hat{h}_2(z_2)$, and $\hat{h}_3(z_3)$ denote the output of the FWNs.
  No prior knowledge about the unknown dynamics of the network and no off-line learning are required. Furthermore, the network initialization is done arbitrarily and then, all parameters of the network are adjusted by the adaptive laws (20), (29) and (38). Then, the dead-zone operator-based model is used to describe the saturation nonlinearity. The virtual and actual control inputs are applied as

$$\begin{aligned} v_2 &= -\ k_1e_1 - \hat{h}_1(z_1) \\ v_3 &= -\ k_2e_2 - \hat{h}_2(z_2) \\ v &= -\ k_3e_3 - \hat{h}_3(z_3) + \int_0^{50}\hat{\rho}_\lambda(r,t)\mathrm{d}z_r(v)\mathrm{d}r \end{aligned} \tag{43}$$

  where $\int_0^{50}\hat{\rho}_\lambda(r,t)\mathrm{d}z_r(v)\mathrm{d}r$ is approximated by

$$\int_0^{50}\hat{\rho}_\lambda(r,t)\mathrm{d}z_r(v)\mathrm{d}r \cong \sum_{i=1}^{500}\hat{\rho}_\lambda(i\Delta r,t)\Delta r \tag{44}$$

Journal : Large 40815 | Dispatch : 20-6-2018 | Pages : 19
Article No. : 515 | LE | TYPESET
MS Code : IJFS-D-17-00702 | CP | DISK

Table 1 Comparison results between the NIP and LIP approximators

Approximator	Criteria	$h_1(z_1)$	$h_2(z_2)$	$h_3(z_3)$
NIP approximator	RMSE	0.2970	3.7612	5.0804
	Number of nodes	2	3	3
	Number of adjustable parameters	6	21	21
LIP approximator	RMSE	0.8674	5.0233	6.0412
	Number of nodes	20	150	150
	Number of adjustable parameters	20	150	150

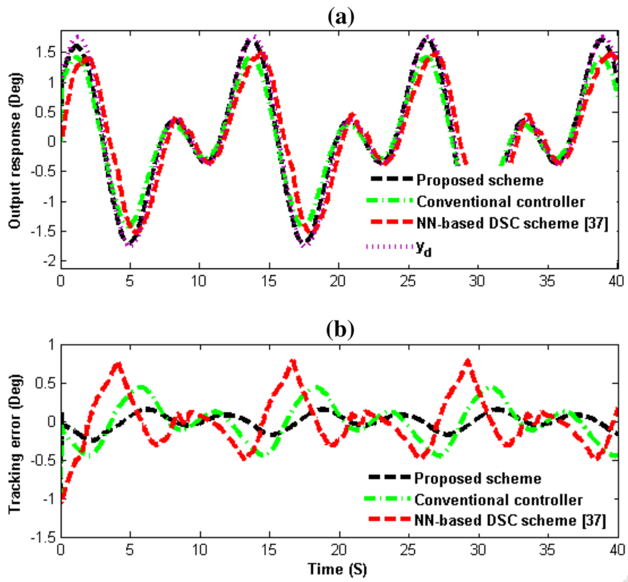

Fig. 5 **a** Output response, **b** tracking error (Case 1)

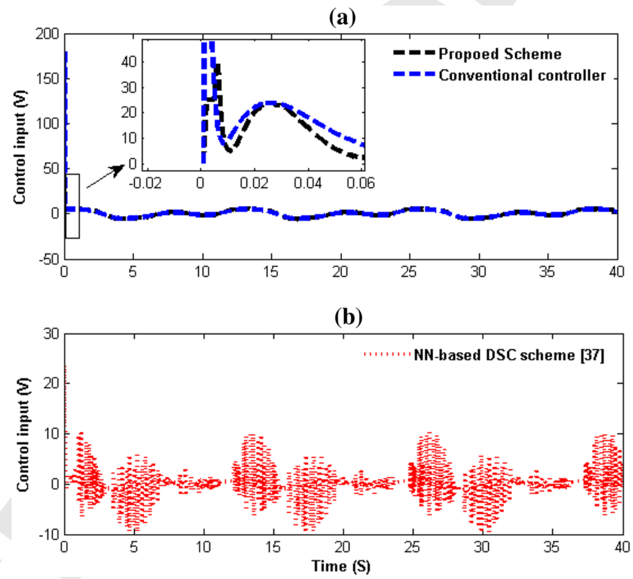

Fig. 6 Control input (Case 1) **a** the proposed scheme and conventional controller, **b** NN-based DSC scheme [37]

and $\Delta r = 0.1$. Other design parameters are set to $k_1 = 5.5$, $k_2 = 5$, $k_3 = 4.5$, $\tau = 0.01$, $\gamma_1 = 5$, $\gamma_2 = \gamma_3 = 3$, $\gamma_p = 0.1$. Also, the initial conditions are set to zero.

- *The conventional controller*

  The conventional controller indicates the FWN-based DSC controller which is designed for uncertain nonlinear system (1) without considering input saturation. In this controller, the constructed adaptive FWN is invoked to represent the model of the unknown functions and then the DSC controller is designed using the proposed FWN model. The virtual and actual control inputs by the conventional controller are proposed as

$$\begin{aligned} v_2 &= -k_1 e_1 - \hat{h}_1(z_1) \\ v_3 &= -k_2 e_2 - \hat{h}_2(z_2) \\ v &= -k_3 e_3 - \hat{h}_3(z_3) \end{aligned} \tag{45}$$

  The design parameters k_1, k_2, k_3, τ, the learning rates γ_1, γ_2, γ_3, and the FWN models were chosen as the same as the proposed controller in this work.

- *NN-Based DSC Controller* [37]

  The proposed NN-based DSC controller in [37] is applied for uncertain nonlinear system (42) in the presence of input saturation. It uses radial-basis-function neural network to approximate the unknown functions and then it designs DSC scheme. It uses linear-in-parameter approximator, and it only adjusts the weights of the network. Furthermore, the saturation nonlinearity is approximated by the tanh function that requires the bound of the input saturation. The controller design parameters were chosen according to [37].

In the following, the simulations are presented for two cases.

Case 1 Tracking response for sinusoidal desired trajectory

Journal : Large 40815 | Dispatch : 20-6-2018 | Pages : 19
Article No. : 515 | LE | TYPESET
MS Code : IJFS-D-17-00702 | CP | DISK

To illustrate the effectiveness of the proposed controller, the time-varying desired trajectory is taken as $y_d = \sin t + \cos(0.5t)$.

In order to show that the proposed NIP approximator solves the "cure of dimensionality" problem, radial-basis-function neural network as a LIP approximator was invoked to approximate uncertain functions $h_1(z_1)$, $h_2(z_2)$ and $h_3(z_3)$. The results are shown in Fig. 4. Also, comparison results between the NIP and LIP approximators are shown in Table 1. Table 1 reports the root mean square error (RMSE), number of nodes and number of adjustable parameters for both of NIP and LIP approximators. As it is seen from the reported results, the NIP approximator achieves less RMSE than the LIP one by using less number of nodes and adjustable parameters. In comparison with the LIP approximator, the NIP approximators achieve better approximation accuracy by using less number of adjustable parameters. So, it can avoid the "curse of dimensionality" problem.

Table 2 Computation time for different values of Δr for one typical sampling time

Δr cases	$\Delta r = 0.1$	$\Delta r = 0.01$	$\Delta r = 0.001$
Case 1	0.005698 S	0.036116 S	0.197894 S
Case 2	0.005821 S	0.044435 S	0.202674 S

Output response and tracking error of the proposed controller and other methods are shown in Fig. 5.

From Fig. 5a, the output of the system is able to track the desired position trajectory in the presence of the uncertain dynamics and unknown saturation nonlinearity; also, it has better steady-state behaviour than the other methods. The tracking error for each scheme is shown in Fig. 5b. It is seen that the tracking error tends to sufficiently small neighbourhood of the origin and remains there while the control signal is not large and the

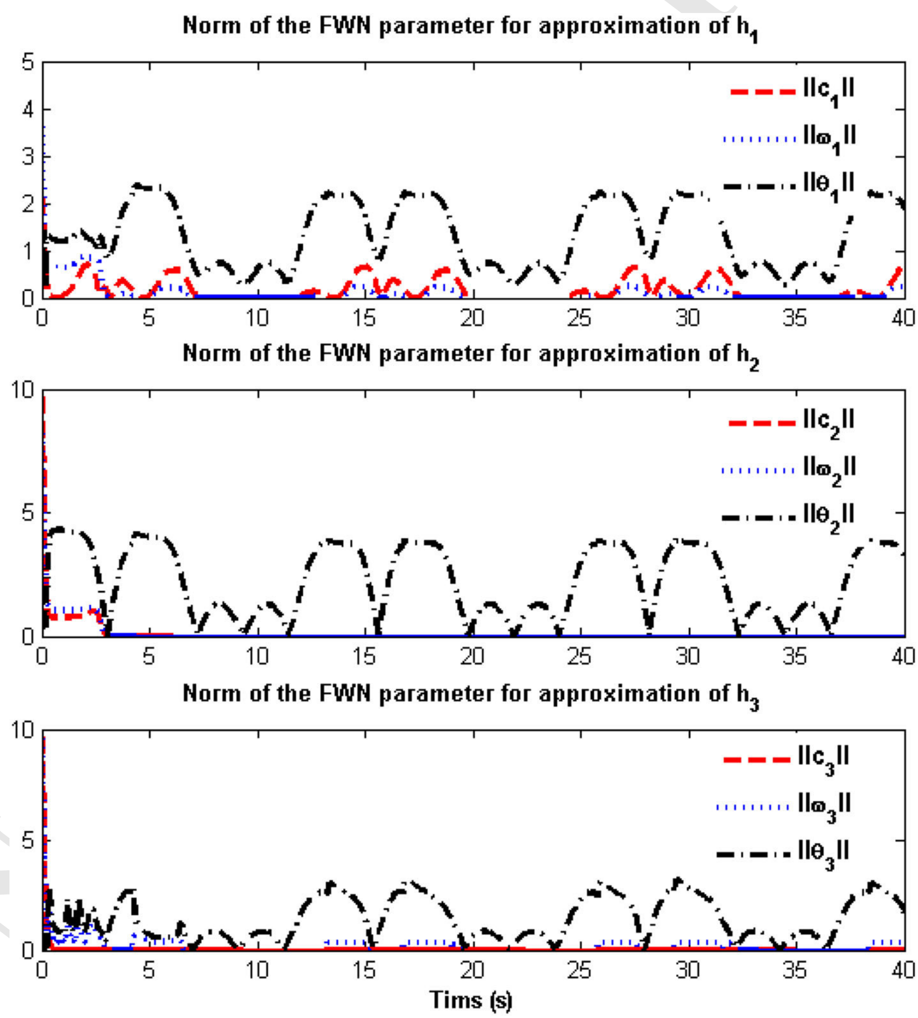

Fig. 7 Norm of the FWN parameters (Case 1)

Journal : Large 40815 | Dispatch : 20-6-2018 | Pages : 19
Article No. : 515 | LE | TYPESET
MS Code : IJFS-D-17-00702 | CP | DISK

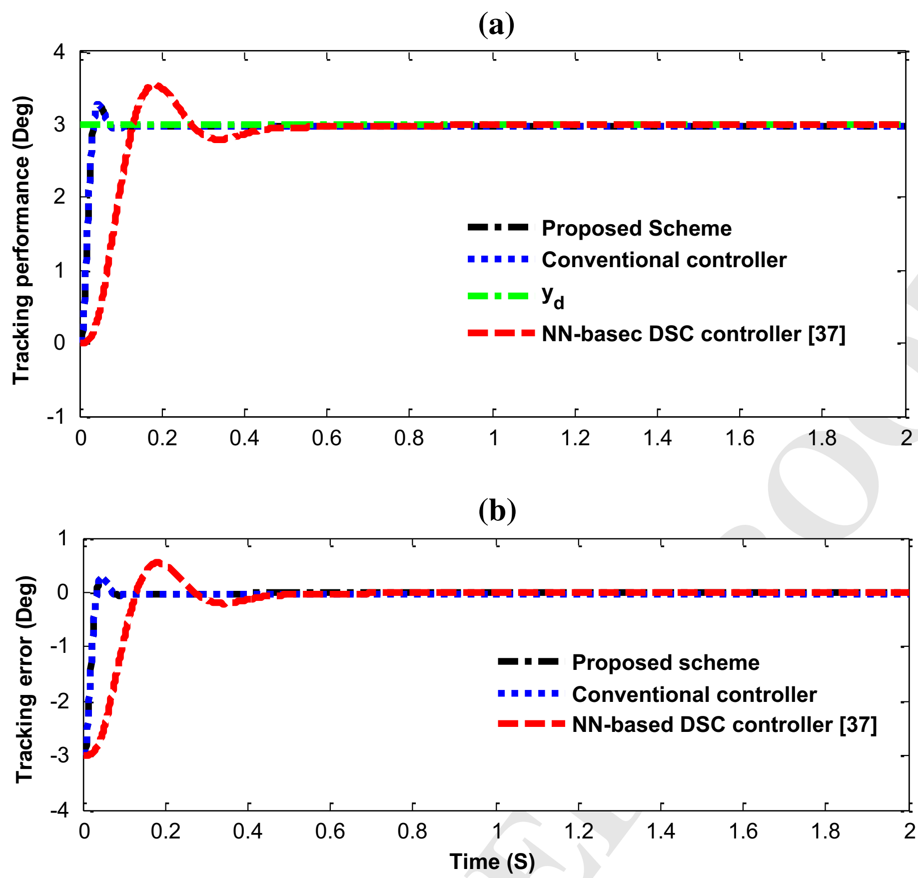

Fig. 8 **a** Output response. **b** Tracking error (Case 2)

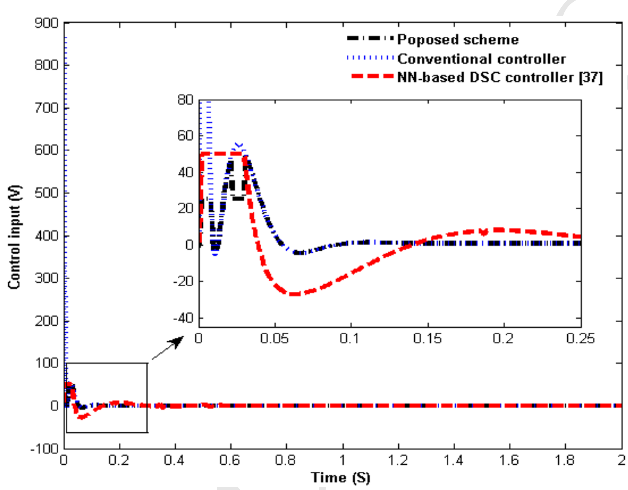

Fig. 9 Control input (Case 2)

singularity problem has been eliminated. The tacking performance obtained in Fig. 5 shows that the proposed scheme has compensated the effect of the unknown saturation nonlinearity and has been able to model the unknown dynamics of the system without any prior knowledge or off-line computation.

The control effort for each scheme is shown in Fig. 6. It is seen from the simulation results in Fig. 6 that the proposed scheme has less amplitude than the conventional one. Further, it has better behaviour and less fluctuation than the proposed scheme in [37]. As it is seen from Fig. 6b, the control effort of the proposed scheme in [37] has many fluctuations that make its implementation hard.

Also, integral term $\int_0^{50} \hat{\rho}_{\lambda}(r,t)\mathrm{d}z_r(v)\mathrm{d}r$ in the control input (43) is approximated by summation term $\sum_{i=1}^{M} \hat{\rho}_{\lambda}(i\Delta r,t)\Delta r$; small values of Δr result in better estimation of integral term. However, it requires more

Journal : Large 40815 | Dispatch : 20-6-2018 | Pages : 19
Article No. : 515 | ☐ LE | ☐ TYPESET
MS Code : IJFS-D-17-00702 | ☑ CP | ☑ DISK

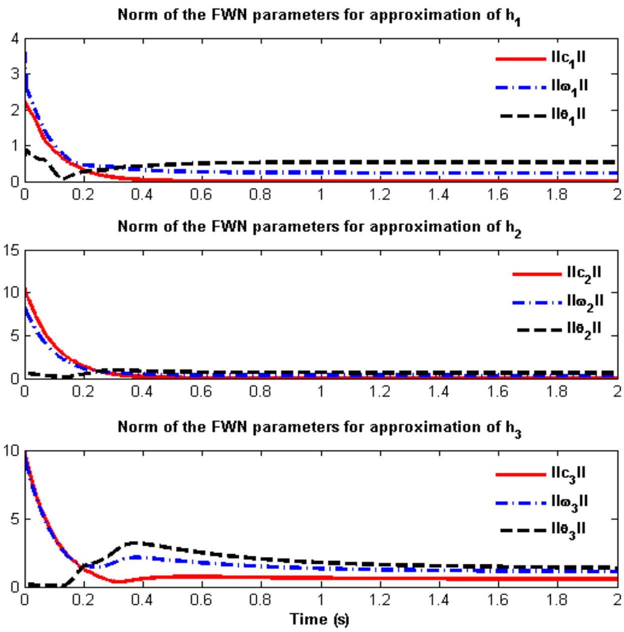

Fig. 10 Norm of the FWN parameters (Case 2)

computation. Computation time for different values of Δr for the two cases considered in this work (Case 1 and Case 2) was reported in Table 2. It should be noted that the reported results in Table 2 approximate the integral term $\int_0^{50} \hat{\rho}_\lambda(r,t)\mathrm{d}z_r(v)\mathrm{d}r$ by $\sum_{i=1}^{M} \hat{\rho}_\lambda(i\Delta r,t)\Delta r$ just for one typical sampling time. One sampling time has been selected for simplicity, and it does not affect the generality of the discussion. As it is obvious from Table 2, smaller values of Δr require larger computation time.

Also, Fig. 7 shows the norm of the FWN parameters such as dilation and translation of the wavelet functions and the weights of the network. Reported results show that the norm of the adjustable parameters is bounded.

Case 2 Tracking constant desired trajectory

To illustrate the effectiveness of the proposed scheme, the desired position trajectory is assumed to be constant and it is chosen as $y_d = 3$. The simulation results are shown in Figs. 8, 9 and 10. Figure 8a shows the angular position of the link (y) and the desired position (y_d). The position tracking error is depicted in Fig. 8b. From Fig. 8, good

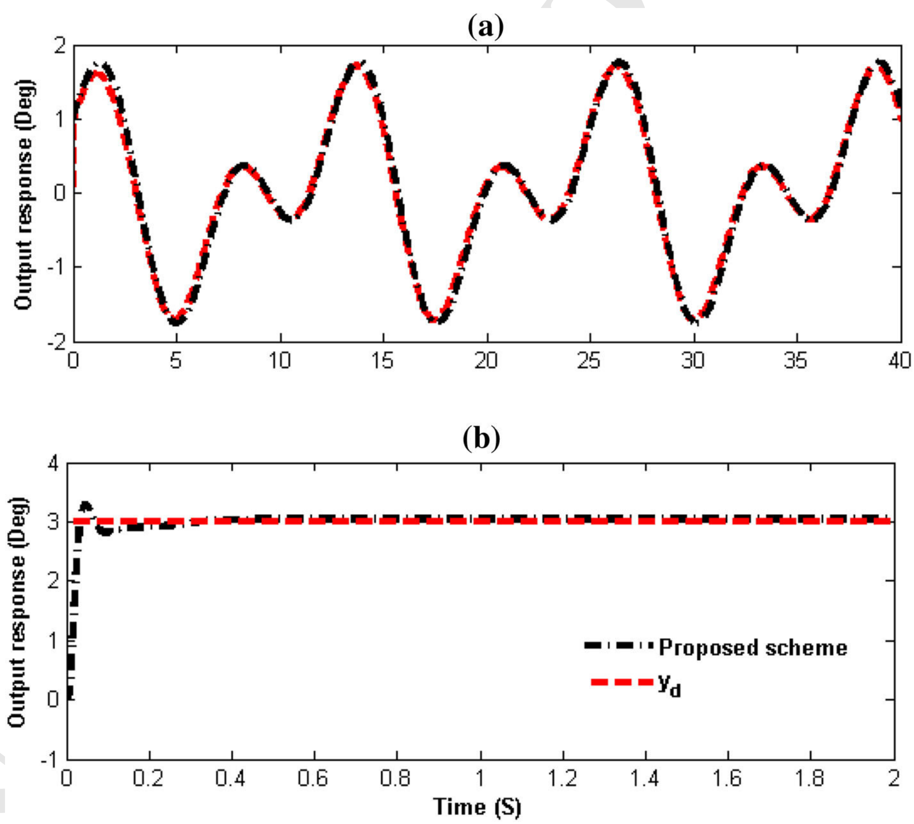

Fig. 11 Output response of the proposed scheme in the presence of disturbance: **a** Case 1, **b** Case 2

Journal : Large 40815 | Dispatch : 20-6-2018 | Pages : 19
Article No. : 515 | LE | TYPESET
MS Code : IJFS-D-17-00702 | CP | DISK

tracking performance is inferred for uncertain system (1) in the presence of uncertain dynamics and input saturation. Furthermore, the proposed scheme improves the characteristics of the transient response, significantly. It eliminates the undesirable overshoot and reduces the settling time. From Fig. 8, the output response and the tracking error of the proposed scheme match to the output response and the tracking error of the conventional controller. This verifies the ability of the proposed scheme to compensate the effect of the saturation nonlinearity.

The control input is shown in Fig. 9. It is inferred from Fig. 9 that the control input is limited to the saturation bound. The reported results demonstrate that the control energy of the proposed scheme is smaller than that of the other methods. Finally, the norm of the adjustable parameters of the FWN is shown in Fig. 10. The boundedness of the norm of the FWN parameters including the translation and dilation parameters of wavelets and weights of the network are inferred from the reported results in Fig. 10.

Finally, the robustness of the proposed scheme is checked by adding external disturbances $d(t) = 0.4\cos(2t)$ to the input of the control system. The results for Cases 1 and 2 are presented in Fig. 11. Figure 11a, b shows the results for tracking of sinusoidal desired trajectory and constant desired trajectory, respectively. The results verify that the proposed scheme can achieve tracking and regulation performance in the presence of external disturbance. So, the obtained results demonstrate the robustness of the proposed scheme against external disturbance.

6 Conclusion

A dead-zone operator-based dynamic surface control scheme was developed for uncertain strict-feedback nonlinear systems in the presence of the input saturation. Adaptive fuzzy wavelet network as a nonlinear-in-parameter approximator is used to model the unknown dynamics of the system without any prior knowledge or off-line learning. Saturation constraint is modelled using the dead-zone operator-based model that does not require the bound of saturation being known. Using the adaptive fuzzy wavelet network approximator and the dead-zone operator-based saturation model, an adaptive dynamic surface control is developed. Stability analysis guarantees that all signals of the closed-loop system are uniformly ultimately bounded and the tracking error can be arbitrarily made small by proper selection of design parameters. The proposed scheme avoids the "explosion of complexity" and "curse of dimensionality" problems. Furthermore, it avoids the singularity problem that is conventional problem in the nonlinear systems with uncertain control gains. Simulation results demonstrate the effectiveness of the proposed scheme. Implementation of the proposed scheme for the real-world applications can be considered as a future work. Also, two other issues are suggested for future works: (1) extending the proposed control approach to the uncertain nonlinear systems with time delay and input saturation and (2) designing an adaptive fuzzy wavelet network-based output feedback control for the considered system.

Acknowledgements This research is carried out under the Grant Number 141/632 of the Shahrekord University.

Appendix A: Proof of Theorem 1

In this section, proof of Theorem 1 is presented. To analysis the stability, the following Lyapunov function candidate is considered:

$$\begin{aligned} V = &\sum_{i=1}^{n-1}\left(\frac{1}{2g_i}e_i^2 + \frac{1}{2}\eta_{i+1}^2\right) \\ &+ \sum_{i=1}^{n}\left(\frac{1}{2\gamma_1}\tilde{\boldsymbol{\theta}}_i^{\mathrm{T}}\tilde{\boldsymbol{\theta}}_i + \frac{1}{2\gamma_2}\tilde{\mathbf{c}}_i^{\mathrm{T}}\tilde{\mathbf{c}}_i + \frac{1}{2\gamma_3}\tilde{\boldsymbol{\omega}}_i^{\mathrm{T}}\tilde{\boldsymbol{\omega}}_i\right) + \frac{1}{2\beta}e_n^2 \\ &+ \frac{1}{2\gamma_\rho}\int_0^R \tilde{\rho}_\lambda^2(r,t)\mathrm{d}r \end{aligned} \tag{A1}$$

where $\tilde{\rho}_\lambda(r,t) = \rho_\lambda(r) - \hat{\rho}_\lambda(r,t)$, $\tilde{\boldsymbol{\theta}}_i = \boldsymbol{\theta}_i^* - \hat{\boldsymbol{\theta}}_i$, $\tilde{\mathbf{c}}_i = \mathbf{c}_i^* - \hat{\mathbf{c}}_i$ and $\tilde{\boldsymbol{\omega}}_i = \boldsymbol{\omega}_i^* - \hat{\boldsymbol{\omega}}_i$. Differentiating (A1) with respect to time results in:

$$\begin{aligned} \dot{V} = &\sum_{i=1}^{n-1}\left(\frac{1}{g_i}e_i\dot{e}_i - \frac{\dot{g}_i e_i^2}{2g_i^2} + \eta_{i+1}\dot{\eta}_{i+1}\right) + \frac{1}{\beta}e_n\dot{e}_n \\ &- \sum_{i=1}^{n}\left(\frac{1}{\gamma_1}\tilde{\boldsymbol{\theta}}_i^{\mathrm{T}}\dot{\hat{\boldsymbol{\theta}}}_i + \frac{1}{\gamma_2}\tilde{\boldsymbol{c}}_i^{\mathrm{T}}\dot{\hat{\boldsymbol{c}}}_i + \frac{1}{\gamma_3}\tilde{\boldsymbol{\omega}}_i^{\mathrm{T}}\dot{\hat{\boldsymbol{\omega}}}_i\right) - \frac{\dot{\beta}}{2\beta^2}e_n^2 \\ &- \frac{1}{\gamma_\rho}\int_0^R \tilde{\rho}_\lambda(r,t)\frac{\partial}{\partial t}\hat{\rho}_\lambda(r,t)\mathrm{d}r \end{aligned} \tag{A2}$$

Substituting (22), (31) and (39) into (A2) results in:

Journal : Large 40815 | Dispatch : 20-6-2018 | Pages : 19
Article No. : 515 | □ LE | □ TYPESET
MS Code : IJFS-D-17-00702 | ☑ CP | ☑ DISK

$$\begin{aligned}\dot{V} = &\sum_{i=1}^{n-1}\left(e_i(e_{i+1}+\eta_{i+1}-k_ie_i+\tilde{h}_i)-\frac{\dot{g}_ie_i^2}{2g_i^2}+\eta_{i+1}\dot{\eta}_{i+1}\right)\\ &+e_n\left(-k_ne_n+\int_0^R(\hat{\rho}_\lambda(r,t)-\rho_\lambda(r))\mathrm{d}z_r(v)\mathrm{d}r+\tilde{h}_n\right)\\ &-\sum_{i=1}^{n}\left(\frac{1}{\gamma_1}\tilde{\boldsymbol{\theta}}_i^{\mathrm{T}}\dot{\hat{\boldsymbol{\theta}}}_i+\frac{1}{\gamma_2}\tilde{\mathbf{c}}_i^{\mathrm{T}}\dot{\hat{\mathbf{c}}}_i+\frac{1}{\gamma_3}\tilde{\boldsymbol{\omega}}_i^{\mathrm{T}}\dot{\hat{\boldsymbol{\omega}}}_i\right)-\frac{\dot{\beta}}{2\beta^2}e_n^2\\ &-\frac{1}{\gamma_\rho}\int_0^R\tilde{\rho}_\lambda(r,t)\frac{\partial}{\partial t}\hat{\rho}_\lambda(r,t)\mathrm{d}r\end{aligned}\tag{A3}$$

Let us define $\tilde{\boldsymbol{\psi}}_i=\boldsymbol{\psi}_i^*-\hat{\boldsymbol{\psi}}_i$. Now, $\tilde{h}_i$ can be written as [50]

$$\tilde{h}_i=\tilde{\boldsymbol{\theta}}_i^{\mathrm{T}}\hat{\boldsymbol{\psi}}_i+\hat{\boldsymbol{\theta}}_i^{\mathrm{T}}\tilde{\boldsymbol{\psi}}_i+\tilde{\boldsymbol{\theta}}_i^{\mathrm{T}}\tilde{\boldsymbol{\psi}}_i+\delta_i^*\tag{A4}$$

where $i=1,\ldots,n$. Adaptive FWN is used as a NIP approximator, so the basis function $\boldsymbol{\psi}_i$ has nonlinear dependencies to the adjustable parameters of the network. Therefore, to develop the adaptive learning laws for tuning the network parameters, the Taylor expansion linearization technique is employed to transform the nonlinear function into a partially linear form [48, 50]. The result is obtained as

$$\tilde{\boldsymbol{\psi}}_i=A_i^{\mathrm{T}}\tilde{\boldsymbol{\omega}}_i+B_i^{\mathrm{T}}\tilde{\mathbf{c}}_i+o_i\tag{A5}$$

where $i=1,\ldots,n$, $A_i=\left(\frac{\partial\boldsymbol{\psi}_i}{\partial\boldsymbol{\omega}_i}\right)\Big|_{\boldsymbol{\omega}_i=\hat{\boldsymbol{\omega}}_i}$, $B_i=\left(\frac{\partial\boldsymbol{\psi}_i}{\partial\mathbf{c}_i}\right)\Big|_{\mathbf{c}_i=\hat{\mathbf{c}}_i}$ and o_i is the high-order terms of expansion. Substituting (A5) into (A4) gives:

$$\tilde{h}_i=\tilde{\boldsymbol{\theta}}_i^{\mathrm{T}}\hat{\boldsymbol{\psi}}_i+\hat{\boldsymbol{\theta}}_i^{\mathrm{T}}\left(A_i^{\mathrm{T}}\tilde{\boldsymbol{\omega}}_i+B_i^{\mathrm{T}}\tilde{\mathbf{c}}_i\right)+\tilde{\boldsymbol{\theta}}_i^{\mathrm{T}}\tilde{\boldsymbol{\psi}}_i+\hat{\boldsymbol{\theta}}_i^{\mathrm{T}}o_i+\delta_i^*\tag{A6}$$

Also, substituting (23), (32) and (A6) into (A3) results in:

$$\begin{aligned}\dot{V}=&-\sum_{i=1}^{n-1}\left(k_i+\frac{\dot{g}_i}{2g_i^2}\right)e_i^2-\left(k_n+\frac{\dot{\beta}}{2\beta^2}\right)e_n^2\\ &+\sum_{i=1}^{n-1}e_i(e_{i+1}+\eta_{i+1})+\sum_{i=1}^{n}e_i\left(\tilde{\boldsymbol{\theta}}_i^{\mathrm{T}}(A_i^{\mathrm{T}}\tilde{\boldsymbol{\omega}}_i+B_i^{\mathrm{T}}\tilde{\mathbf{c}}_i+o_i)\right)\\ &+\sum_{i=1}^{n}e_i\left(\tilde{\boldsymbol{\theta}}_i^{\mathrm{T}}\hat{\boldsymbol{\psi}}_i+\hat{\boldsymbol{\theta}}_i^{\mathrm{T}}(A_i^{\mathrm{T}}\tilde{\boldsymbol{\omega}}_i+B_i^{\mathrm{T}}\tilde{\mathbf{c}}_i)+\hat{\boldsymbol{\theta}}_i^{\mathrm{T}}o_i+\delta_i^*\right)\\ &+\sum_{i=1}^{n-1}\left(-\frac{\eta_{i+1}^2}{\tau_{i+1}}+\eta_{i+1}M_{i+1}\right)-\sum_{i=1}^{n}\left(\frac{1}{\gamma_1}\tilde{\boldsymbol{\theta}}_i^{\mathrm{T}}\dot{\hat{\boldsymbol{\theta}}}_i+\frac{1}{\gamma_2}\tilde{\mathbf{c}}_i^{\mathrm{T}}\dot{\hat{\mathbf{c}}}_i+\frac{1}{\gamma_3}\tilde{\boldsymbol{\omega}}_i^{\mathrm{T}}\dot{\hat{\boldsymbol{\omega}}}_i\right)\\ &+e_n\left(\int_0^R(\hat{\rho}_\lambda(r,t)-\rho_\lambda(r))\mathrm{d}z_r(v)\mathrm{d}r\right)\\ &-\frac{1}{\gamma_\rho}\int_0^R\tilde{\rho}_\lambda(r,t)\frac{\partial}{\partial t}\hat{\rho}_\lambda(r,t)\mathrm{d}r\end{aligned}\tag{A7}$$

Since $\hat{\boldsymbol{\theta}}_i^{\mathrm{T}}A_i^{\mathrm{T}}\tilde{\boldsymbol{\omega}}_i=\tilde{\boldsymbol{\omega}}_i^{\mathrm{T}}A_i\hat{\boldsymbol{\theta}}_i$ and $\hat{\boldsymbol{\theta}}_i^{\mathrm{T}}B_i^{\mathrm{T}}\tilde{\mathbf{c}}_i=\tilde{\mathbf{c}}_i^{\mathrm{T}}B_i\hat{\boldsymbol{\theta}}_i$, (A7) is rewritten as:

$$\begin{aligned}\dot{V}=&-\sum_{i=1}^{n-1}\left(k_i+\frac{\dot{g}_i}{2g_i^2}\right)e_i^2-\left(k_n+\frac{\dot{\beta}}{2\beta^2}\right)e_n^2\\ &+\sum_{i=1}^{n-1}e_i(e_{i+1}+\eta_{i+1})+\sum_{i=1}^{n-1}\left(-\frac{\eta_{i+1}^2}{\tau_{i+1}}+\eta_{i+1}M_{i+1}\right)\\ &+\sum_{i=1}^{n}\tilde{\boldsymbol{\theta}}_i^{\mathrm{T}}\left(\left(\hat{\boldsymbol{\psi}}_i-A_i^{\mathrm{T}}\hat{\boldsymbol{\omega}}_i-B_i^{\mathrm{T}}\hat{\mathbf{c}}_i\right)e_i-\frac{1}{\gamma_1}\underline{\boldsymbol{\theta}}_i\right)\\ &+\sum_{i=1}^{n}\tilde{\boldsymbol{\omega}}_i^{\mathrm{T}}\left(A_i\hat{\boldsymbol{\theta}}_ie_i-\frac{1}{\gamma_3}\underline{\boldsymbol{\omega}}_i\right)+\sum_{i=1}^{n}\tilde{\mathbf{c}}_i^{\mathrm{T}}\left(B_i\hat{\boldsymbol{\theta}}_ie_i-\frac{1}{\gamma_2}\hat{\mathbf{c}}_i\right)\\ &+\sum_{i=1}^{n}e_i\left(\tilde{\boldsymbol{\theta}}_i^{\mathrm{T}}\left(A_i^{\mathrm{T}}\boldsymbol{\omega}_i^*+B_i^{\mathrm{T}}\mathbf{c}_i^*\right)+\boldsymbol{\theta}_i^{*\mathrm{T}}o_i+\delta_i^*\right)\\ &-\frac{1}{\gamma_\rho}\int_0^R\tilde{\rho}_\lambda(r,t)\left(\frac{\partial}{\partial t}\hat{\rho}_\lambda(r,t)+\gamma_\rho e_n\mathrm{d}z_r(v)\right)\mathrm{d}r\end{aligned}\tag{A8}$$

Let us define $\Delta_i=\tilde{\boldsymbol{\theta}}_i^T\left(A_i^T\boldsymbol{\omega}_i^*+B_i^T\mathbf{c}_i^*\right)+\boldsymbol{\theta}_i^{*T}o_i+\delta_i^*$ for $i=1,\ldots,n$. Substituting adaptive laws (20), (29) and (38) into (A8) results in:

$$\begin{aligned}\dot{V}=&-\sum_{i=1}^{n-1}\left(k_i+\frac{\dot{g}_i}{2g_i^2}\right)e_i^2-\left(k_n+\frac{\dot{\beta}}{2\beta^2}\right)e_n^2\\ &+\sum_{i=1}^{n-1}e_i(e_{i+1}+\eta_{i+1})+\sum_{i=1}^{n-1}\left(-\frac{\eta_{i+1}^2}{\tau_{i+1}}+\eta_{i+1}M_{i+1}\right)\\ &+\sum_{i=1}^{n}\sigma\tilde{\boldsymbol{\theta}}_i^{\mathrm{T}}\hat{\boldsymbol{\theta}}_i+\sum_{i=1}^{n}\sigma\tilde{\boldsymbol{\omega}}_i^{\mathrm{T}}\hat{\boldsymbol{\omega}}_i+\sum_{i=1}^{n}\sigma\tilde{\mathbf{c}}_i^{\mathrm{T}}\hat{\mathbf{c}}_i+\sum_{i=1}^{n}e_i\Delta_i\\ &+\sigma_\rho\int_0^R\hat{\rho}_\lambda(t,r)\tilde{\rho}_\lambda(r,t)\mathrm{d}r\end{aligned}\tag{A9}$$

Considering the following facts

$$\begin{aligned}&e_ie_{i+1}\le 0.5\left(e_i^2+e_{i+1}^2\right),\quad i=1,2,\ldots,n\\ &e_i\eta_{i+1}\le 0.5\left(e_i^2+\eta_{i+1}^2\right),\quad i=1,2,\ldots,n-1\\ &\left|\eta_{i+1}M_{i+1}\right|\le 0.5\varepsilon\eta_{i+1}^2+0.5\varepsilon^{-1}\bar{M}_{i+1}^2,\quad i=1,2,\ldots,n-1\\ &e_i\Delta_i\le 0.5\left(e_i^2+\bar{\Delta}_i^2\right),\quad i=1,2,\ldots n\\ &\tilde{\rho}_\lambda(r,t)p\le 0.5\tilde{\rho}_\lambda^2(r,t)+0.5p_{\lambda_{\max}}^2\end{aligned}\tag{A10}$$

where $\rho_\lambda(r)\le\rho_{\lambda\max}$, and ε is a positive constant. Also, considering the following inequalities

$$\begin{aligned}&\tilde{\boldsymbol{\omega}}_i^{\mathrm{T}}\hat{\boldsymbol{\omega}}_i\le 0.5\left(\boldsymbol{\omega}_i^{*\mathrm{T}}\boldsymbol{\omega}_i^*-\tilde{\boldsymbol{\omega}}_i^{\mathrm{T}}\tilde{\boldsymbol{\omega}}_i\right),\quad i=1,2,\ldots,n\\ &\tilde{\mathbf{c}}_i^{\mathrm{T}}\hat{\mathbf{c}}_i\le 0.5\left(\mathbf{c}_i^{*\mathrm{T}}\mathbf{c}_i^*-\tilde{\mathbf{c}}_i^{\mathrm{T}}\tilde{\mathbf{c}}_i\right),\quad i=1,2,\ldots,n\\ &\tilde{\boldsymbol{\theta}}_i^{\mathrm{T}}\hat{\boldsymbol{\theta}}_i\le 0.5\left(\boldsymbol{\theta}_i^{*\mathrm{T}}\boldsymbol{\theta}_i^*-\tilde{\boldsymbol{\theta}}_i^{\mathrm{T}}\tilde{\boldsymbol{\theta}}_i\right),\quad i=1,2,\ldots,n\end{aligned}\tag{A11}$$

Now, using (A10) and (A11), (A9) is written as

Journal : Large 40815 | Dispatch : 20-6-2018 | Pages : 19
Article No. : 515 | LE | TYPESET
MS Code : IJFS-D-17-00702 | CP | DISK

$$\begin{aligned}\dot{V} \le & -\left(k_1 - \frac{g_1^d}{2g_{l1}^2} - 1.5\right)e_1^2 - \sum_{i=2}^{n-1}\left(k_i - \frac{g_i^d}{2g_{li}^2} - 2\right)e_i^2 \\ & -\left(k_n - \frac{\beta^d}{2\beta_l^2} - 1\right)e_n^2 - \sum_{i=1}^{n-1}\left(\frac{1}{\tau_{i+1}} - 0.5\varepsilon - 0.5\right)\eta_{i+1}^2 \\ & + 0.5\sigma\sum_{i=1}^{n}\left(\bar{\theta}_i^2 + \bar{c}_i^2 + \bar{\omega}_i^2\right) + 0.5\sum_{i=1}^{n-1}\left(\bar{\Delta}_i^2 + \varepsilon^{-1}\bar{M}_{i+1}^2\right) \\ & -0.5\sigma\sum_{i=1}^{n}\left(\tilde{\boldsymbol{\theta}}_i^{\mathrm{T}}\tilde{\boldsymbol{\theta}}_i + \tilde{\mathbf{c}}_i^{\mathrm{T}}\tilde{\mathbf{c}}_i + \tilde{\boldsymbol{\omega}}_i^{\mathrm{T}}\tilde{\boldsymbol{\omega}}_i\right) \\ & \sigma_\rho\int_0^R\left(0.5\tilde{\rho}_\lambda^2(r,t) - 0.5p_{\lambda_{\max}}^2\right)\mathrm{d}r\end{aligned} \tag{A12}$$

Choose the deign parameters k_i, τ_{i+1}, σ and σ_ρ such that $k_1 - \frac{g_1^d}{2g_{l1}^2} - 1.5 > 0$, $k_i - \frac{g_i^d}{2g_{li}^2} - 2 > 0$, $i = 2,\ldots,n-1$, $k_n - \frac{\beta^d}{2\beta_l^2} - 1 > 0$, $\frac{1}{\tau_{i+1}} - 0.5\varepsilon - 0.5 > 0$, $\sigma > 0$ and $\sigma_\rho > 0$, respectively.

Considering the design parameters k_i, τ_{i+1}, σ and σ_ρ, comparing (A12) with (A1) reveals that (A12) satisfies the following inequality

$$\dot{V} \le -\alpha V + \beta \tag{A13}$$

where α and β are as follows:

$$\alpha \le \min\left(\begin{matrix} 2g_{h1}\left(k_1 - 1.5 - \frac{g_1^d}{2g_{l1}^2}\right) \\ 2g_{hi}\left(k_i - 2 - \frac{g_i^d}{2g_{li}^2}\right) \\ 2\beta_h\left(k_n - 1 - \frac{\beta^d}{2\beta_l^2}\right) \\ \frac{2}{\tau_{i+1}} - \varepsilon - 1 \\ \sigma\gamma_1, \sigma\gamma_2, \sigma\gamma_2 \\ \sigma_\rho\gamma_\rho \end{matrix}\right)$$

$$\begin{aligned}\beta = & \ 0.5\sum_{i=1}^{n-1}\left(\bar{\Delta}_i^2 + \varepsilon^{-1}\bar{M}_{i+1}^2\right) + 0.5\sigma\sum_{i=1}^{n}\left(\bar{\theta}_i^2 + \bar{c}_i^2 + \bar{\omega}_i^2\right) \\ & + 0.5\sigma_\rho R p_{\lambda_{\max}}^2\end{aligned}$$

Solving inequality (A13) results in:

$$0 \le V \le \frac{\beta}{\alpha} + \left(V(0) - \frac{\beta}{\alpha}\right)e^{-\alpha t} \tag{A14}$$

From (A14), it is obtained that $\lim_{t\to\infty} V = \frac{\beta}{\alpha}$. So, V is bounded by $\frac{\beta}{\alpha}$. Therefore, all signals of the closed-loop system, i.e. e_i, η_{i+1}, $\tilde{\boldsymbol{\theta}}_i$, $\tilde{\boldsymbol{c}}_i$, $\tilde{\boldsymbol{\omega}}_i$ and $\tilde{\rho}_\lambda$ are uniformly ultimately bounded. From the considered Lyapunov function in (A1), it can be inferred that

$$\frac{1}{2g_1}\, e_1^2 \le V \tag{A15}$$

Considering Assumption 2, Eq. (A15) is written as

$$e_1^2 \le 2g_{h1}V \tag{A16}$$

which results in the following bound

$$|e_1(t)| \le \sqrt{2g_{h1}V} \tag{A17}$$

Now, considering (A14), the following bound is obtained for the tracking error

$$|e_1| \le \sqrt{2g_{h1}\left(e^{-\alpha t}V(0) + \frac{\beta}{\alpha}\left(1 - e^{-\alpha t}\right)\right)} \tag{A18}$$

It is seen form (A18) that the bound of the tracking error can be made arbitrarily small by proper selection of the design parameters.

References

1. Jang, J.O.: Neuro-fuzzy networks saturation compensation of DC motor systems. Mechatronics **19**, 529–534 (2009)
2. Yu, C., Xiang, X., Zhang, Q., Xu, G.: Adaptive fuzzy trajectory tracking control for an under-actuated autonomous underwater vehicle subject to actuator saturation. Int. J. Fuzzy Syst. (2007). https://doi.org/10.1007/s40815-017-0396-9
3. Chu, Z., Xiang, X., Zhu, D., Luo, C., Xie, D.: Adaptive sliding mode driving control for autonomous underwater vehicle with input saturation. Int. J. Fuzzy Syst. (2017). https://doi.org/10.1007/s40815-017-0390-2
4. Li, S., Wang, Y., Tan, J.: Adaptive and robust control of quadrator aircrafts with input saturation. Nonlinear Dyn. **89**, 225–265 (2017)
5. Song, Z., Li, H., Sun, K.: Adaptive dynamic surface control for MEMS triaxial gyroscope with nonlinear inputs. Nonlinear Dyn. **78**, 173–182 (2014)
6. Perez-Arancibia, N.O., Tsao, T.-C., Gibson, J.S.: Saturation-induced instability and its avoidance in adaptive control of hard disk drives. IEEE Trans. Control Syst. Technol. **18**, 368–382 (2010)
7. He, W., Dong, Y., Sun, C.: Adaptive neural impedance control of a robotic manipulator with input saturation. IEEE Trans. Syst. Man Cybern. **46**, 334–344 (2006)
8. Lu, K., Xia, Y., Yu, C., et al.: Finite-time tracking control of rigid spacecraft under actuator saturations and faults. IEEE Trans. Autom. Sci. Eng. **13**, 368–381 (2016)
9. Xiang, X., Yu, C., Zhang, Q.: Robust fuzzy 3D path following for autonomous underwater vehicle subject to uncertainties. Comput. Oper. Res. **84**, 165–177 (2017)
10. Yang, J., Tong, S.: Observer-based output-feedback control design for a class of nonlinear switched T–S fuzzy systems with actuator saturation and time delay. Int. J. Fuzzy Systs. **19**, 1333–1343 (2017)
11. Gassara, H., Hajjaji, A.-E., Chaabane, M.: Control of time delay polynomial fuzzy model subject to actuator saturation. Int. J. Fuzzy Syst. **18**, 763–772 (2016)

Journal : Large 40815 | Dispatch : 20-6-2018 | Pages : 19
Article No. : 515 | LE | TYPESET
MS Code : IJFS-D-17-00702 | CP | DISK

12. Rang, M., Wang, Q., Dong, C.: Stabilization of a class of nonlinear systems with actuator saturation via active disturbance rejection control. Automatica **63**, 302–310 (2016)
13. Zhao, F., Ge, S.S., Tu, F., et al.: Adaptive neural network control for active suspension system with actuator saturation. IET Control Theory Appl. **10**, 1696–1705 (2016)
14. Adetola, V., Adn, D.D., Guay, M.: Adaptive model predictive control for constrained nonlinear systems. Syst. Control Lett. **58**, 320–326 (2009)
15. Hu, Q., Ma, G., Xie, L.: Robust and adaptive variable structure output feedback control of uncertain systems with input nonlinearity. Automatica **44**, 552–559 (2008)
16. Shieh, C.S.: Design of three-dimensional missile guidance law with tunable nonlinear H_{∞} control with saturation constraint. IET Control Theory Appl. **3**, 756–763 (2007)
17. Moreno, J.C., Guzmán, J.L., Baños, A., et al.: The input amplitude saturation problem in QFT: a survey. Annu. Rev. Control **35**, 34–55 (2011)
18. Wen, C., Zhou, J., Liu, Z., et al.: Robust adaptive control of uncertain nonlinear systems in the presence of input saturation and external disturbance. IEEE Trans. Autom. Control **56**, 1672–1678 (2011)
19. Peng, Z., Wen, G., Yang, S., Rahmani, A.: Distributed consensus-based formation control for non holonomic wheeled mobile robots using adaptive neural networks. Nonlinear Dyn. **86**, 605–622 (2016)
20. Chen, M., Ge, S.S., Ren, B.: Adaptive tracking control of uncertain MIMO nonlinear systems with input constraints. Automatica. **47**, 452–465 (2011)
21. Wang, D., Huang, J.: Neural network-based adaptive dynamic surface control for a class of uncertain nonlinear systems in strict feedback form. IEEE Trans. Neural Netw. **16**, 195–202 (2005)
22. Yang, X., Liu, D., Huang, Y.: Neural-network-based online optimal control for uncertain nonlinear continuous-time systems with control constraints. IET Control Theory Appl. **7**, 2037–2047 (2013)
23. Xiang, X., Yu, C., Lapierre, L., Zhang, J., Zhang, Q.: Survey on fuzzy-logic-based guidance and control of marine surface vehicles and underwater vehicles. Int. J. Fuzzy Syst. **20**, 572–586 (2018)
24. Liu, H., Pan, Y., Li, S., Chen, Y.: Adaptive fuzzy backstepping control of fractional-order nonlinear systems. IEEE Trans. Syst. Man Cybern. Syst. **47**, 2209–2217 (2017)
25. Liu, H., Li, S., Cao, J., Li, G., Alsaedi, A., Alsaadi, F.E.: Adaptive fuzzy prescribed performance controller design for a class of uncertain fractional-order nonlinear systems with external disturbance. Neurocomputing. **219**, 422–430 (2017)
26. Pan, Y., Yu, H.: Biomimetic hybrid feedback feedforward neural-network learning control. IEEE Trans. Neural. Netw. Learn. Syst. **28**, 1481–1487 (2017)
27. Lu, H., Liu, C., Coombes, M., et al.: Online optimisation-based backstepping control design with application to quadrotor. IET Control Theory Appl. **10**, 1601–1611 (2016)
28. Chen, W., Ge, S.S., Wu, J., et al.: Globally stable adaptive backstepping neural network control for uncertain strict-feedback systems with tracking accuracy known a prior. IEEE Trans. Neural. Netw. Learn. Syst. **26**, 1842–1854 (2015)
29. Wang, H.Q., Chen, B., Liu, X.P., et al.: Robust adaptive fuzzy tracking control for pure-feedback stochastic nonlinear systems with input constraints. IEEE Trans. Cybern. **43**, 2093–2104 (2013)
30. Liu, Z., Lai, G., Zhang, Y., Chen, C.L.P.: Adaptive fuzzy tracking control of nonlinear time-delay systems with dead-zone output mechanism based on a novel smooth model. IEEE Trans. Fuzzy Syst. **23**, 1998–2011 (2015)
31. Liu, Z., Lai, G., Zhang, Y., Chen, X., Chen, C.L.P.: Adaptive neural control for a class of nonlinear time-varying delay systems with unknown hysteresis. IEEE Trans. Neural. Netw. Learn. Syst. **25**, 2129–2140 (2014)
32. Swaroop, D., Hedrick, J.K., Yip, P.P.: Dynamic surface control for a class of nonlinear systems. IEEE Trans. Autom. Control **45**, 1893–1899 (2000)
33. Pan, Y., Yu, H.: Composite learning from adaptive dynamic surface control. IEEE Trans. Autom. Control. **61**, 2603–2609 (2016)
34. Pan, Y., Sun, T., Liu, Y., Yu, H.: Composite learning from adaptive backstepping neural network control. Neural Netw. **95**, 134–142 (2017)
35. Pan, Y., Sun, T., Yu, H.: Composite adaptive dynamic surface control using online recorded data. Int. J. Robust Nonlinear Control **26**, 3921–3936 (2016)
36. Ma, J., Zheng, Z., Li, P.: Adaptive dynamic surface control of a class of nonlinear systems with unknown direction control gains and input saturation. IEEE Trans. Cybern. **45**, 728–741 (2015)
37. Chen, M., Tao, G., Jiang, B.: Dynamic surface control using neural networks for a class of uncertain nonlinear systems with input saturation. IEEE Trans. Neural netw. Learn. Syst. **26**, 2086–2097 (2015)
38. Ma, J., Ge, S.S., Zheng, Z., et al.: Adaptive NN control of a class of nonlinear systems with asymmetric saturation actuators. IEEE Trans. Neural Netw. Learn. Syst. **26**, 1532–1538 (2015)
39. Li, Y., Tong, S., Li, T.: Composite adaptive fuzzy output feedback control design for uncertain nonlinear strict-feedback systems with input saturation. IEEE Trans. Cybern. **45**, 2299–2308 (2015)
40. Gao, S., Ning, B., Dong, H.: Fuzzy dynamic surface control for uncertain nonlinear systems under input saturation via truncated adaptation approach. Fuzzy Sets Syst. **290**, 100–117 (2015)
41. Mousavi, S.H., Khayatian, A.: Dead-zone model based adaptive backstepping control for a class of uncertain saturated systems. Asian J. Control. **18**, 1395–1405 (2016)
42. Liao, F., Luo, Q., Ji, H., et al.: Guidance laws with input saturation and nonlinear robust H_{∞} observers. ISA Trans. **63**, 20–31 (2016)
43. Chen, M., Shi, P., Lim, C.C.: Robust constrained control for MIMO nonlinear systems based on disturbance observer. IEEE Trans. Autom. Control **60**, 3281–3286 (2016)
44. Yan, X., Chen, M., Wu, Q., et al.: Dynamic surface control for a class of stochastic nonlinear systems with input saturation. IET Control Theory Appl. **10**, 35–43 (2016)
45. Barron, A.R.: Universal approximation bounds for superpositions of a sigmoidal function. IEEE Trans. Inf. Theory. **39**, 930–945 (1993)
46. Farrell, J.A., Polycarpou, M.M.: Adaptive approximation based control. Wiley, Hoboken (2006)
47. Ho, D.W.C., Zhang, P.-A., Xu, J.: Fuzzy wavelet network for function learning. IEEE Trans. Fuzzy Syst. **9**, 200–211 (2001)
48. Lin, C.-K.: Nonsingular terminal sliding mode control of robot manipulators using fuzzy wavelet networks. IEEE Trans. Fuzzy Syst. **14**, 849–859 (2006)
49. Carrol, J.J., Dawson, D.M.: Integrator backstepping techniques for the tracking control of permanent magnet brush DC motors. IEEE Trans. Ind. Electron. **31**, 248–255 (1995)

Journal : Large 40815 Dispatch : 20-6-2018 Pages : 19
Article No. : 515 □ LE □ TYPESET
MS Code : IJFS-D-17-00702 ☑ CP ☑ DISK

50. Shahriari-kahkeshi, M., Sheikholeslam, F.: Adaptive fuzzy wavelet network for robust fault detection and diagnosis in nonlinear systems. IET Control Theory Appl. **8**, 1487–1498 (2014)

Maryam Shahriari-Kahkeshi received her M.S. and Ph.D. degrees in control engineering from Isfahan University of Technology, Isfahan, Iran, in 2010 and 2014, respectively. Since 2014, she has been an Assistant Professor in the Faculty of Engineering at Shahrekord University. Her research activities are focused on system identification, multi-agent systems and control of nonlinear systems with input nonlinearities.

Journal : Large 40815 | Dispatch : 20-6-2018 | Pages : 19
Article No. : 515 | ☐ LE | ☐ TYPESET
MS Code : IJFS-D-17-00702 | ☑ CP | ☑ DISK